UNIVERSITÉ KASDI MERBAH OUARGLA

FACULTÉ DE MATHÉMATIQUES
ET DES SCIENCES DE LA MATIÈRE

DÉPARTEMENT DE PHYSIQUE

Order number:

Serial number:

THÈSE DE DOCTORAT

Filière: Physique

Spécialité: Matière et Rayonnement

par

BEN NANA YASMINA

HYDRODYNAMICS OF LASER WELDING OF METAL ALLOYS PLATES AND ELECTRONIC BROADENING

Thèse soutenenue le : 11/04/2021 devant le jury composé de:

PR: A. BOUKRAA	PROFESSEUR	U. Ouargla	Président
PR: S. DOUIS	PROFESSEUR	U. Ouargla	Examinateur
PR: K. CHENINI	PROFESSEUR	U. Ghardaïa	Examinateur
PR: M. DIFALLAH	PROFESSEUR	U. El-Oued	Examinateur
DR: L. BENMEBROUK	MCA	U. Ouargla	Examinateur
PR: F. KHELFAOUI	PROFESSEUR	U. Ouargla	Rapporteur

April 11th, 2021

Dedication

To my:

- mother

- father

- husband

- chidren

-friends

- all familly

- colleagues at Department of Physic at University Kasdi Merbah of Ouargla

I didecate this work.

Acknowledgement

Firstly thanks go to ***Allah*** *before and after Who enabled me to complete this work.*

I would like to express my deep gratitude to ***Prof. Khelfaoui. Fethi****, for supervisor constructive criticism, help and guidance and patience. I could not complete my thesis without their enlightening instruction.*

Special thanks to ***Prof. A. Boukraa*** *for agreeing to be president of jury of this thesis.*

I also thank ***Prof. S. Douis****,* ***Prof. K. Chenini****,* ***Prof. M. Difallah*** *and* ***Dr. L. Benmebrouk*** *for being part for my jury members.*

I would like to thank ***Prof. Meftah Mohammed Tayeb****, for their support during my Ph.D. study. and their enlightening instruction, impressive kindness and patience.*

I am also grateful to ***Dr. Lemkeddem Soumaia****,* ***Dr. Ballah Zakia****, for their help in my study and patient advice's. I would also to thank all my friends in the laboratory LRPPS, where I have done this work.*

I am sincerely grateful to my ***parents*** *and my* ***husband****. They encouraged me and listened to me during all the difficult moments. I want to thank my* ***sisters****, my* ***brothers****, and all the other family members. Thank you for consistently encouraging me to be brave, independent and optimistic, and I appreciate their support and love in these years.*

Finally but not least. I also express thanks to all the other ***professors****,* ***researchers*** *and* ***secretaries*** *who have helped me in the past years.*

Contents

List of Figures

List of Tables

Liste of Symbols

Greek Symbols

α_d	Polarizability of neutral [Å^3]
$\Delta\lambda_D$	Doppler width, Debye's length [Å]
γ_D	Doppler broadening [cm^{-1}]
γ_L	Pressure broadening [cm^{-1}]
$\lambda(T)$	Thermal conductivity [$\frac{W}{(m.K)}$]
λ_0	Central wavelength[Å]
μ_{in}	Ion mobility coefficients of the background gas mixture[$cm^2.V^{-1}.s^{-1}$]
ν_{ij}	Frequency of transition from a level of principal quantum number i to j [$1/s$]
Ω	Molecular properties characteristic of the interacting particles [-]
$\rho(T)$	Gas density [$\frac{Kg}{m^3}$]
σ_{12}	Collision distance [Å]
ε_{12}	Energy of interaction[eV]

Roman Symbols

$\hbar$	Planck's constant [$cm^2.g.s^{-1}$]
A	Ion broadening parameter [-]
a_0	Bohr radius [A]
A_{ji}	Atomic transition probability[$1/s$]
A_r	Preex ponential factor [cm^3/s]
c	Speed of light [cm/s]
C_6	Interaction constant
$C_p(T)$	Specific heat [$\frac{KJ}{(Kg.K)}$]
D	Diffusion coefficient measured [cm^2/s]
$D_{e,M}$	Diffusion constant of neutral particle molecules [cm^2/s]
E	Electric field [V/cm]
e	Electric charge[C]
E^*	Excitation energy [eV]

E_a Activation energy $[eV]$

E_c Kinetic energy $[eV]$

E_{ion} Ionisation energy $[eV]$

E_i Energy of principal quantum number i $[eV]$

E_j Energy of quantum number j $[eV]$

f_{ij} Oscillator strength [-]

g_j Statistical weigh of quantum states (j)[-]

I_0 Total line intensity $[Watt.m^{-3}.Sr]$

I_λ Specific intensity at wavelength λ $[Watt.m^{-3}.Sr]$

J_i Angular momentum of the state i [-]

J_m Angular momentum of the lower state among the sublevels i and j [-]

k_B Boltzmann's constant $[eV/K]$

k_r Rate coefficient $[cm^3/s]$

m Atomic mass $[amu]$

m_e Electron mass $[g]$

$N(n)$ Total number of molecules $[cm^{-3}]$

$N_{1,2}$ Particle number densities (numbers of molecules) $[cm^{-3}]$

N_e Electron density $[cm^{-3}]$

N_e^{ref} Reference electron density $[cm^{-3}]$

N_i Ion density in $[cm^{-3}]$

N_j number per unit volume (number density)$[cm^{-3}]$

N_o Population density of the ground state$[cm^{-3}]$

P Pressure$[atm]$

$R_{e,p}$ Source term $[cm^{-3}/s]$

R_{ij} Transition matrix element [-]

T Absolute temperature $[K]$

T_a Atomic excitation temperature $[K]$

T_e Electron temperature $[K]$

T_g Gas temperature $[K]$

T_i Ion temperature $[K]$

U_o Partition function[-]

V_c Critical velocity $[cm/s]$

v_c Reduced critical velocity [-]

v_s Velocity of the particle along the line of sight s $[cm/s]$

v_{th} Most probable velocity of the particles $[cm/s]$

General introduction

Low temperature plasma physics is a very active area of research located on the boundaries between physics, chemistry and materials science. Recent technological developments have led to a revived interest in plasma physics and technology.

Laser welding can be done at atmospheric pressure in the presence of air or in the presence of a shielding gas under forced or non-forced speed. Atmospheric pressure gas attracts extensive attention because of its low cost and simplified operation in comparison with low pressure gas. Nitrogen and oxygen are the major constituents of air, so it is important to investigate the dynamic of nitrogen and oxygen mixture gases at atmospheric pressure.

Nitrogen and/or oxygen at atmospheric pressure has been demonstrated in a number of previous studies, like Wang yi-Nan et al. in (2013) and Wang yi-Nan and L. Yue in (2017) [1, 2]. Physical systems naturally evolve toward higher entropy states. Hence, thermal diffusion is a direct result of the logical operation of the universe [3].

In this thesis, we focus on the effect of surface welded by laser at dynamic thermal diffusion in air mixture by calculating the gas, ions and electron temperatures and densities, which becomes (the surface) a point source of thermal waves. The model used in this work has been simplified because of the multi-chemical processes and multi-particles in the air.

Dynamics of heat transfer have been illustrated and measured in many experimental and theoretical research, e.g; M. C. Sullivan et al. in (2007) [4] have measured temperature in metal rod as a function of position and time, and used simple heat flow equations in order to extract the thermal diffusion of the metal.

Gfroerer et al. in (2015) [3] have measured time-dependent radial temperature profiles of a heated rod generate a temperature gradient in the center of a metallic plate in real time via the video feed from a thermal camera. They estimated the thermal diffusivity , which is used to confirm the accuracy of the finite-difference (FDM) simulations.

In many processes, such as the arc welding and laser welding, a luminous gas plasma forms near the weld pool. In welding, the luminosity of the plasmas is a very important property. Many experimental research studied and analyzed the light emission spectra from the plasma produced by laser welding to get information about plasma parameters (N_e, T_e) by the Boltzmann plot and/or Stark broadening method, like Hoffman et al. in (2006) [5,6]; they studied the plasma produced during laser welding of magnesium alloy.

We describe simple method [7] to calculation Stark broadening using the impact theory which takes into account non adiabatic effects due to electron collisions. We neglect the contribution of ions to the broadening of isolated lines. The corresponding profiles are, therefore, of dispersion (Lorentz-

Weisskopf) type. Because of the long-range nature of the (dipole-monopole) interaction between emitting atoms and perturbing electrons, perturbation theory can be used to calculate the dominant terms in widths and shifts of these dispersion profiles. We apply this theory to the isolated neutral lines of magnesium. The isolated lines are the lines whose half-width is much smaller than the separation between the perturbed level and the next interacting level. Practically all the broadening is caused by interactions between the upper state of the line in question and its neighbors, and lower state interactions can be neglected [7].

Consequently, a number of experimental and theoretical papers have dealt with Stark broadening of both neutral atom and ion spectral lines.

Freudenstein and Cooper (1978) [8] derived a simple formula for estimating Stark widths of neutral lines; this formula gives the correct trend of Stark width dependence upon electron temperature. Dimitrijević and Sahal-Bréchot (1994) [9] presented results of semi-classical calculations of Stark broadening parameters for some lines of heavy neutral atoms. Dimitrijević and Konjević (1986) [10] estimated simple formulae for Stark widths and shifts of neutral atom lines based on the simple method of Freudenstein Cooper and the GBKO semi-classical theory. In 1994, Dimitrijević and Sahal-Bréchot [9] used a semi-classical approach to calculate impact line widths and shifts for 267 Mg I multiplets caused by electron, proton and other ion as a function of temperature and perturber density [9]. B. Zmerli et al. (2008) [11]have analyzed the temperature dependence of Stark widths for neutral atom spectral lines. Sahal-Bréchot et al. (2011) [12] have calculated a great number of data, obtained through the impact semi-classical perturbation theory. They are currently implemented in the STARK-B database [13], which participates in the European effort within the Virtual Atomic and Molecular Data Center [13].

In chapter 1, we present the main elements relating to the main themes addressed (Fundamental equations of the fluid model, equilibrium laws and spectral line profiles in plasmas).

In chapter 2, we have established (1D) fluid model contains a set of gas dynamics equations, to describe the heat transfer by convection evolution. The coupled equations for plasma gas temperature, electron temperature, charged and neutral species densities were solved simultaneously.

In chapter 3, we present a theoretical implementation to obtain the minimum of the impact parameter for strong and weak contribution in collision operator. We also present the contribution of strong collision and weak collision respectively for magnesium neutral emitters.

In chapter 4, spatial and temporal distributions of species (N_2, O_2, N_2^+, O_2^+ and electrons and temperatures) are presented and discussed.

In chapter 5, we present the calculated full Stark width (ionic and electronic) of isolated lines Mg I, Be I and Ca I. We present and discuss a comparison between our result with the theoretical and the experimental results of Griem (1974) [14], STARK-B web site [13], Dimitrijević and Sahal-Bréchot (1994) results [9], we calculate stark broadening of Mg I under welding conditions. Finally, we present a conclusion and some perspectives

Chapter 1

Theoretical foundations of gaseous media near weld surfaces and spectral line shapes of radiative transitions

1.1 Introduction

The laser welding process has received significant attentions in recent years [15]. The effectiveness of laser welding depends greatly on the physical properties of the material to be welded [16]. As the lightest structural material available, magnesium alloys are widely used in aerospace, automotive, electronics and other fields for advantages such as specific strength, good castability, excellent machinability and recyclability [6]. Two main types of lasers, CO_2 and Nd:YAG with wavelengths of 10.6 and 1.06μm, respectively, have been used to investigate the weldability of material alloys in many experiments. The CO_2 laser has high power output, high efficiency, proven reliability and safety. With the recent development of high output power, the improvement of beam quality and the possibility of glass fiber delivery, the Nd:YAG laser has entered the fields dominated by the CO_2 laser. The weldability of magnesium alloys was reported to be significantly better with the Nd:YAG laser due to its shorter wavelength, which in turn reduced the threshold irradiance required for keyhole mode welding and produced a more stable weld pool. Compared with CO_2 lasers, Nd:YAG laser beams have a higher welding efficiency [16]. In addition, for the particular physical properties of magnesium alloys, low melting point ($650°C$), low boiling point ($1090°C$) and low ionization energy ($7.6eV$), there are some particular phenomena of magnesium plasma under the action of a laser beam. So it is of great interest to investigate the characteristics of magnesium welding plasma [6].

Laser welding method heats locally and gives welds of very high quality. The interaction of the laser beam with the metal vapor leads to a partial ionization which forms a plasma composed of ionized vapors inside the keyhole and on the weld pool [17].

During laser welding near-surface plasma is not stable, it constantly changes its position in relation to the area of introduction of the beam into the welding covering. In this case, the plasma has no screening effect which confirms that the nature of formation of the welded joint is the same along the entire length of the welded joint [18].

The laser beam welding operation is done in the presence of atmospheric gas (O_2/N_2) or in the presence of protective gas which gives better quality to the weld [19].

An important area of scientific research is the investigation of wall kinetic processes in low pressure gases and plasmas, since the interaction of different atomic and molecular species with walls can significantly influence the gas phase concentration of these species. To investigate the influence of surfaces on the densities of gas phase species the transfer of these species to or from the surface must be studied [20].

In the presence of protective gas, convection phenomena are very important [19]; equations of the fluid model allow to calculate the velocities of these gases and to study the general dynamics. Within our team, Master works were interested in the calculation of these velocities [21, 22]. The study of the properties of gases near the welding surfaces can be done by a diagnosis of the spectral lines. We can cite as examples the works on spectral line shapes of Cu and Mg, [5, 23–27]

The shape of spectral lines in plasmas is a topic of wide-ranging interest and the subject of study for many years. The two major line broadening mechanisms in the laser plasma are Doppler broadening and Pressure broadening. The latter includes broadening by collisions with foreign species, Resonance broadening and Stark broadening and shift [28]. When line shapes and shifts are used for plasma diagnostic purposes, in most of the cases, one cannot change plasma conditions so the contribution of other broadening mechanisms has to be carefully estimated and, if necessary, measured widths and shifts corrected [29].

In this chapter we present theoretical foundations of atmospheric gas (O_2 / N_2) near weld surfaces to determine densities and temperatures of the gas species. The considered species are O_2, N_2, O_2^+, N_2^+ and electrons.

We also present in this chapter a quick reminder on the calculation of spectral lines in plasma.

1.2 Gas reactions

There is sufficient background radiation in the atmosphere creating electrons such that the free electron concentration is $10^{-2}cm^{-3}$ to the gas number density at standard pressure and temperature of $10^{20}cm^{-3}$. The free electrons will be accelerated by the resulting electric field. Along the way, they collide with the interstitial gas atoms or molecules (M).

These collisions represent three groups of chemical reactions:

Elastic : $e^- + M \rightarrow e^- + M$,

Excitation: $e^- + M \rightarrow e^- + M^*$ if $e \geq E^*$,
Ionization: $e^- + M \rightarrow 2e^- + M^+$ if $e \geq E_{ion}$,

Note that for the excitation and ionization reactions, the kinetic energy of the incident electron E_c must be greater than or equal to the minimum energy required for excitation E^* or ionization E_{ion}, respectively.

1. $E_c \geq E^*_{min}$,
2. $E_c \geq E_{ion}$,

1.2.1 Elastic Collisions

The elastic collision is the dominant type of collisions and can occur for any kinetic energy of the incident electron E_c. The electron and molecule collide like two billiard balls, and all the energy of the collision is maintained (for the most part) as kinetic energy that is, kinetic energy is conserved. In these binary (two-body) collisions, the electron is moving much faster than the molecule, and therefore the gas molecule is typically considered at rest. The electron collides with the molecule and takes or at a new trajectory.

1.2.2 Excitation Collisions

The electrons of an atom or a molecule are linked and they have discrete energies. Depending on the collision process, an incident electron can have an elastic collision with the atom or the molecule by exciting or de-exciting a bonded electron. In this case there is no conservation of kinetic energy; on the other hand there is conservation of the total energy of the system.

1.2.3 Ionization Collisions

At sufficient kinetic energy, a free electron may actually cause an electron to detach from the neutral resulting in a second free electron and a positive ions. The energy required for this reaction is called the ionization energy E_{ion}. Therefore the incident free electron must have a kinetic energy of $E_c \geq E_{ion}$ to create an ion. This is called electron-impact ionization [30].

1.2.4 Electronic recombination

In a gas, atomic processes are equilibrium reactions. If there are ionization reactions by electrons, there would be reverse reactions of electronic recombination.

1.2.5 Dissociation reaction

Collisions of electrons with molecules can dissociate these molecules and give lighter radicals or atoms. The kinetic energy of the electrons must be greater than the activation energy E_a of the reaction.
In table 1.1, we present some important collision processes in oxygen and nitrogen mixture in plasma.

We have limited ourselves to the reactions giving the different species of our study.
The constant k_r presents rate coefficient of each reaction. The Arrhenius form of the rate constant as a function of temperature is [31, 32]:

$$k_r = A_r T^{\beta} exp(\frac{-E_a}{k_B T}), \tag{1.1}$$

For general equilibrium reaction, as :

$aA + bB \rightleftharpoons cC + dD,$

The rate consumption (or production) R takes the form [32]:

$\frac{d}{dt}[A] = -k_{r1}[A]^a[B]^b + k_{r2}[C]^c[D]^d,$
$R = -k_{r1}[A]^a[B]^b + k_{r2}[C]^c[D]^d.$

Table 1.1 presents the main reactions in oxygen and nitrogen mixture in plasma.

Table 1.1 – *Important collision processes in oxygen and nitrogen mixture in plasma.*

No.	Reaction	Rate coefficient cm^3/s	Ref
1	$e + N_2 \rightarrow e + 2N$	$k_1 = 5.4 \times 10^{-4} \left(\frac{T_e}{300}\right)^{-1.6} \exp(-\frac{9.76}{T_e})$	[31]
2	$e + N_2 \rightarrow 2e + N_2^+$	$k_2 = 2.4 \times 10^{-6} T_e^{-0.5} \exp(-\frac{14.6}{T_e})$	[31]
3	$e + O_2 \rightarrow 2e + O_2^+$	$k_3 = 2.34 \times 10^{-9} T_e^{1.03} \exp(-\frac{12.29}{T_e})$	[33]
4	$e + O_2 \rightarrow e + 2O$	$k_4 = 6.86 \times 10^{-9} \exp(-\frac{6.29}{T_e})$	[33]
5	$e + N_2^+ \rightarrow N_2$	$k_5 = 2.8 \times 10^{-7} \sqrt{\frac{300}{T_e}}$	[34]
6	$e + O_2^+ \rightarrow O_2$	$k_6 = 2.1 \times 10^{-7} \sqrt{\frac{300}{T_e}}$	[34]

In table 1.2, we present the production (or consumption) rate R of each species per unit of time and per unit of volume. This term R can present the term "source" in the differential equations relating to the conservation of global quantities (mass, species, energies), where $\Delta\epsilon_r$ are the activation energies related to electronic energy term source $R_{\epsilon e}$.
Table 1.2 presents the term sources for considered species and electronic energy listed in table 1.1.

Table 1.2 – *Term sources for considered species and electronic energy.*

Species	Term sources
R_{N_2}	$-k_1[N_2][N_e] - k_2[N_2][N_e] + k_5[N_2^+][N_e]$
R_{O_2}	$-k_3[O2][N_e] - k_4[N_e][O2] + k_6[O_2^+][N_e]$
$R_{N_2^+}$	$k_2[N_2][N_e] - k_5[N_2^+][N_e]$
$R_{O_2^+}$	$k_3[O_2][N_e] - k_6[O_2^+][N_e]$
R_e	$k_2[N_2][N_e] + k_3[N_e][O_2] - k_5[N_2^+][N_e] - k_6[O_2^+][N_e]$
$R_{\epsilon e}$	$[(\Delta\epsilon_1 K_1 - \Delta\epsilon_2 K_2)[N_2] + (\Delta\epsilon_4 K_4 - \Delta\epsilon_3 K_3)[O_2]][N_e]$

1.3 Mathematical model of statistical properties of gas near weld plates

1.3.1 General models for statistical properties of gas

The study of statistical properties in gas mixtures presenting complex phenomena requires experimental work or numerical work.
The numerical simulation models used in this area are classified into four main families or classes.

Monte Carlo simulations:

The first Monte Carlo Simulation (MCS) model was proposed by Metropolis et al. in 1953 [35]. They are a broad class of computational algorithms that are used to model the probability of different outcomes in a process that cannot easily be predicted due to the intervention of random variables. The underlying concept is to use randomness to solve problems that might be deterministic in principle [36]. Collisions and reactions in gas phase of SiH_4/H_2 mixture used in PECVD (plasma enhanced chemical vapor deposition) process have been simulated by MCS models [37, 38].

Molecular Dynamics Simulation:

Molecular Dynamics Simulation (MDS) model is a computer simulation method for analyzing the physical movements of atoms and molecules. The atoms and molecules are allowed to interact for a fixed period of time, giving a view of the dynamic of the system. In the most common version, the trajectories of atoms and molecules are determined by numerically solving Newton's equations and their potential energies are often calculated using inter atomic potentials or molecular mechanics force fields [36].

Fluid Model:

The plasma fluid model consists of solving Poisson' s equation and one or more moments of Boltzmann' s equation to obtain (for a three moment fluid model) the density, momentum, and energy of each charged species. Each of these equations contains transport coefficients or rate coefficients which represent the effect of collisions and which are input data for the fluid model [39].
J. Hugill and T. Saktioto in (2001) used a fluid model to simulate Nitrogen plasmas at atmospheric pressure produced by 2.45 GHz microwaves [31]. At low electron temperature, this plasma presented dissociation reaction and ionization reaction. Concentrations of species N_2, N, N_2^+, N^+ and electrons were calculated as function of time.
Z. Ballah and F. Khelfaoui in (2018) developed a one dimensional time-dependent fluid model in presence of the magnetic field to simulate argon gas in RF magnetron sputtering discharge [40]. The model is based on continuity equation and electron temperature equation coupled with Poisson's equation. Numerical simulations were resolved by using the Finite Volume Method (FVM) and the Thomas algorithm. The obtained results of electrical properties (electron and ion densities, electrical potential, electric field and electron temperature) were in good agreement with other works.

Hybrid simulation:

Hybrid models have been introduced as a method to speed computations, is a modeling approach that combines two or more simulation models. Belenguer and Boeuf first introduced this method for rf discharges in what is now termed a "beam-bulk" simulation [39].

1.3.2 General Equations of fluid model for densities, temperatures and energy

Among the main equations relating to the fluid model are the continuity, the momentum and the energy equations. We also add to these equations, equations of electromagnetism and equations taking into account collision phenomena or other processes.

The continuity equation for particles can be written as [41]:

$$\frac{\partial N_e}{\partial t} + \nabla J_e = R_e \ , \tag{1.2}$$

$$\frac{\partial N_i}{\partial t} + \nabla J_i = R_i \ , \tag{1.3}$$

$$\frac{\partial N_n}{\partial t} + \nabla J_n = R_n \ , \tag{1.4}$$

Where $N_{e,i,n}$, $J_{e,i,n}$ and $R_{e,i,n}$ represent the densities of species, flux and the source term, respectively. The subscripts (e,i,n) represent electron, ions, neutral, respectively. The particle fluxes under the diffusion approximation are expressed as [41]:

$$J_e = -\mu_e N_e E - D_e \nabla N_e \ , \tag{1.5}$$

$$J_i = -\mu_i N_i E - D_i \nabla N_i \ , \tag{1.6}$$

$$J_n = -D_n \nabla N_n \ , \tag{1.7}$$

Where $D_{e,i,n}$ and $\mu_{e,i,n}$ represent the diffusion coefficient and mobility respectively. In addition, E is the electric field.

The heat equation for continues medium (fluid, solid) can be written as [4]:

$$\frac{\rho(T) C_p(T) \partial T}{\partial t} = \nabla.[\lambda(T) \nabla T] = \frac{\partial}{\partial x}[\lambda(T) \frac{\partial T}{\partial x}] \ , \tag{1.8}$$

Where ρ(T), C_p(T) and λ(T) are Density (in units $\frac{Kg}{m^3}$), Specific heat (in units $\frac{KJ}{(Kg.K)}$) and Thermal conductivity (in units $\frac{W}{(m.K)}$).

The electron-energy balance can be expressed as [41]:

$$\frac{\partial N_e \epsilon_e}{\partial t} + \frac{5}{3} \nabla J_{e\epsilon} = R_{e\epsilon} \ , \tag{1.9}$$

Where: $\epsilon_e = \frac{3}{2} K_B T_e$

In the electron energy equation, T_e is the electron temperature, $J_{e\epsilon}$ is the electron-energy flux , the loss term $R_{e\epsilon}$ is considered as the inelastic collision between electrons and molecules,

The electrical field equation can be written as [41]:

$$\nabla E = \frac{e}{\epsilon_0} \left(\sum_j N_{ij} - N_e \right) \ . \tag{1.10}$$

Where: $e = 1.6 \times 10^{-19}$ C, $\epsilon_0 = 8.85 \times 10^{-14}$ $CV^{-1}cm^{-1}$ are the electric charge, the permittivity of free space.

Table 1.3 presents energy thresholds of the collision processes in oxygen and nitrogen gas mixture in plasma.

Table 1.3 – *Threshold energy* $\Delta\epsilon_r$.

Reaction no.	$\Delta\epsilon(eV)$	Ref
1	8.4	[42]
2	15.4	[42, 43]
3	12.1	[42, 43]
4	5.58	[42, 43]
5	−15.4	[42, 43]
6	−12.1	[42, 43]

1.3.3 Transport coefficients for heat equation

The expression of the heat equations coefficients in $(N_2 - 20\%O_2)$ mixture according to the gas temperature T_g is:

Specific heat:

The general expression of the specific heat for this mixture is [44].

$$C_p(N_2 - 20\%O_2) = 0.8C_p(N_2) + 0.2C_p(O_2) \ , \tag{1.11}$$

where: $C_p(N_2)$ and $C_p(O_2)$ are respectively the specific heat capacities for N_2 and O_2 calculated from the following expressions (in J $mol^{-1}K^{-1}$) as a function of the gas temperature T_g (in K):

$$C_p(N_2) = 29.1 + \frac{2494.2}{553.4\sqrt{\frac{\pi}{2}}} exp\left(-2\left(\frac{T_g - 1047.4}{553.4}\right)^2\right) \ , \tag{1.12}$$

and

$$C_p(O_2) = 28.2 + \frac{6456.2}{788.3\sqrt{\frac{\pi}{2}}} exp\left(-2\left(\frac{T_g - 1006.9}{788.3}\right)^2\right) \ , \tag{1.13}$$

Thermal conductivity:

The thermal conductivity of plasma is the ratio between the heat flux and the corresponding temperature gradient [44–46]. For the mixture $N_2 - 20\%O_2$

$$\lambda(N_2 - 20\%O_2) = 0.8\lambda(N_2) + 0.2\lambda(O_2) \ = \frac{\lambda(N_2)}{1 + \phi_{N_2O_2}\frac{[O_2]}{[N_2]}} + \frac{\lambda(O_2)}{1 + \phi_{O_2N_2}\frac{[N_2]}{[O_2]}} \ , \tag{1.14}$$

where $\phi_{N_2O_2}$ and $\phi_{O_2N_2}$is Wassiljewa coefficients, which were calculated from the expressions presented in [46]. The thermal conductivity of pure N_2 and O_2 given by

$$\lambda(N_2) = 1.717 + 0.084T_g - 1.948 \times 10^{-5}T_g^2 \ , \tag{1.15}$$

and

$$\lambda(O_2) = 1.056 + 0.087T_g - 8.912 \times 10^{-6}T_g^2 \ , \tag{1.16}$$

Density:

According to the general expression of the binary mixture the density is [44, 47].

$$\rho(N_2 - 20\%O_2) = 0.8\rho(N_2) + 0.2\rho(O_2) \ , \tag{1.17}$$

The densities of pure N_2 and O_2, at atmospheric pressure:

$$\rho(N_2) = \frac{348}{T} \ , \tag{1.18}$$

$$\rho(O_2) = \frac{376}{T} \ . \tag{1.19}$$

1.3.4 Transport coefficients for continuity equation

The diffusion in a fluid is the phenomenon of transport of matter in the fluid from the areas of strong concentration towards the areas of weak concentration.

Diffusion coefficient for neutral particles:

Diffusion coefficient for neutral particles is [48].

$$D = \frac{3}{16(N_1 + N_2)\sigma_{12}^2}\sqrt{\frac{2k_BT(m_1 + m_2)}{\pi m_1 m_2}} \ , \tag{1.20}$$

Chapman and Cowling, 1970 accurate a theoretical estimation of gaseous diffusion to an average of about eight percent, leads to the equation

$$D = \frac{1.86 \times 10^{-3}T^{3/2}\sqrt{\frac{1}{m_1} + \frac{1}{m_2}}}{P\sigma_{12}^2\Omega} \ , \tag{1.21}$$

in which the collision distance σ_{12} is given by:

$$\sigma_{12} = \frac{1}{2}(\sigma_1 + \sigma_2) \ , \tag{1.22}$$

The values of σ_1 and σ_2 are listed in Table 1.4.
The molecular properties characteristic of the interacting particles Ω is given by:

$$\Omega = \frac{A}{\Psi B} + \frac{C}{e^{D\Psi}} + \frac{E}{e^{F\Psi}} + \frac{G}{e^{H\Psi}} \ , \tag{1.23}$$

where $\Psi = T_{gas}/\varepsilon_{12}$ and $\varepsilon_{12} = \sqrt{\varepsilon_1.\varepsilon_2}$, values of the energy of interaction $\frac{\varepsilon_{12}}{k_B}$are given in Table 1.4 this energy is a geometric average of contributions from the two species [31, 49, 50].
With $A = 1.06036, B = 0.15610, C = 0.19300, D = 0.47635, E = 1.03587, F = 1.52996, G = 1.76474, H = 3.89411$.
Table 1.4 presents the lennard-Jones potential parameters for Air, N_2 and O_2. The Lennard-Jones potential describes the potential energy of interaction between two non-bonding atoms or molecules based on their distance of separation [32].

Table 1.4 – *Lennard-Jones potential parameters found from viscosities.*

Substance	$\sigma_{12}(A^0)$	$\varepsilon_{12}/k_B\ (K)$
N_2	3.798	71.4
O_2	3.467	106.7

Estimates of σ_{12} and ε_{12} are not available for all gases. Instead, many authors have developed empirical relations like:

$$D = 10^{-3}\frac{T^{1.75}\sqrt{\frac{1}{m_1}+\frac{1}{m_2}}}{P\left[\left(\sum_i V_{i1}\right)^{1/3}+\left(\sum_i V_{i2}\right)^{1/3}\right]^2}\ . \tag{1.24}$$

in which T is in Kelvin. P is in atmospheres. V_{ij} are the volumes of parts of the molecule j. Table 1.5 presents atomic diffusion volumes for N_2, O_2 and Air [49].

Table 1.5 – *Diffusion volumes* $\sum V_{ij}$.

Molecules	$\sum V_{ij}$
N_2	17.9
O_2	16.6

The Diffusion coefficient for a neutral molecule and electron for collisions between an electron of mass m_e and neutral particles of mass m with number density n,becomes

$$\nu_{e,n} = \frac{4}{3}N\pi\sigma_{12}^2\sqrt{\frac{8k_BT}{\pi m_e}}\ , \tag{1.25}$$

Because

$$m_1 \equiv m \gg m_2 \equiv m_e\ , \tag{1.26}$$

The equation 1.25 becomes for air $(N_2 + O_2)$

$$\nu_{e,n} = 5.4\times10^{-10}N\sqrt{T}\ , \tag{1.27}$$

With the use of the relation

$$D_{e,n} = \frac{(m_e+m)k_BT}{m_e m\nu_{e,n}} \simeq \frac{k_BT}{m_e\nu_{e,n}}\ , \tag{1.28}$$

Diffusion coefficient for a neutral molecule and an electron [48]:

$$D_{e,n} = \frac{3k_BT}{4m_eN\pi\sigma_{12}^2}\sqrt{\frac{\pi m_e}{8k_BT}} = \frac{3}{16N\sigma_{12}^2}\sqrt{\frac{2k_BT}{\pi m_e}}\ . \tag{1.29}$$

Diffusion coefficient for charged particles:

The diffusion coefficient D for charged particles is (up to the first approximation)

$$D = \frac{3}{16}\frac{1}{(N_1+N_2)}\sqrt{\frac{2k_BT(m_1+m_2)}{\pi m_1m_2}}\left(\frac{2k_BT}{e^2}\right)^2\frac{1}{A_1(2)}\ , \tag{1.30}$$

where $A_1(2)$ denotes a slowly varying function of T and N_e which will be given later [48].

$$\nu_{+-} = \frac{4}{3}\frac{\pi e^4(N_1m_1+N_2m_2)}{m_1m_2(m_1+m_2)\sqrt{2\pi k_B^3T^3}}A_1(2)\ . \tag{1.31}$$

Diffusion coefficient for neutral particles and positive ions:

The diffusion coefficient of neutral and positive ions is calculated using the Einstein relation,

$$D_{in} = \frac{k_B T_i}{e} \mu_{in} \ , \tag{1.32}$$

The ion temperature T_i which is assumed to be equal to the gas temperature T_g. The ion mobility of ions i in neutral background n is calculated as

$$\mu_{in} = 5.14 \times 10^3 \sqrt{\frac{m_n + m_i}{m_n m_i}} \frac{T_g}{P\sqrt{\alpha_d}} \ . \tag{1.33}$$

The polarizability α_d is tabulated in Table 1.6. The ion mobility in the mixture is again obtained using Blancs law [50].
Table 1.6 presents numerical Value of the Polarizability.

Table 1.6 – *Numerical Value of the Polarizability.*

Species	N_2	O_2	N	O
$\alpha_d(\mathring{A}^3)$	1.76	1.60	1.13	0.15

Diffusion coefficient for electron and positive ions particles:

The electron collision frequency with neutral particles is negligible compared to the collision frequency with positive ions. If we consider the collision frequency of positive ions with respect to an electron,we may use the following conditions: $m_+ \gg m_e$ and $N_+ = N_- + N_e \equiv (1+u)N_e$ where $\frac{N_-}{N_e} = u$ is the ratio of negative ion (N_-) and electron concentrations if the gas as a whole is assumed to be electrically neutral. Then, the general expression 1.31 can be written as:

$$D_{e,+} = \frac{4}{3} \frac{\pi e^4}{\sqrt{2\pi m_e k_B^3 T^3}} A_1(2)(1+u)N_e \ , \tag{1.34}$$

If the number of negative ion is negligible $u << 1, n_+ N_e$ and the electronic collision frequency is proportional to the electronic density, the diffusion coefficient for electron and positive ions is:

$$D_{e,+} = \frac{k_B T}{m_e \nu_{e,+}} = \frac{3}{16} \frac{1}{(1+u)N_e} \sqrt{\frac{2k_B T}{\pi m_e}} \left(\frac{2k_B T}{e^2}\right)^2 \frac{1}{A_1(2)} \ . \tag{1.35}$$

The function $A_1(2)$:

The nature of $A_1(2)$ must be known in order to perform an actual calculation of the collision frequency. This slowly varying function of temperature and density may take different forms depending upon the assumed mean collision distance. The expression given by CHAPMAN and COWLING (1939) is, to the first approximation,

$$A_1(2) = log_e(1 + \nu_{01}^2) \ , \tag{1.36}$$

where

$$\nu_{01} = \frac{4dk_B T}{e^2} \ , \tag{1.37}$$

with d = mean distance between "pairs of neighboring molecules. "If we define d being equal to $(2N_e)^{-1/3}$,

$$A_1(2) = log_e[1 + (\frac{4k_BT}{e^2(2N_e)^{1/3}})^2] \ , \tag{1.38}$$

And if

$$1 \ll \frac{4k_BT}{e^2(2N_e)^{1/3}} \ , \tag{1.39}$$

The correction term $A_1(2)$ is

$$A_1(2) = 2log_e\left(\frac{4k_BT}{e^2(2N_e)^{1/3}}\right) \ , \tag{1.40}$$

If we define d being equal to Debye's length

$$d = \sqrt{\frac{k_BT}{8\pi e^2 N_e}} \ , \tag{1.41}$$

the correction term must be written

$$A_1(2) = log_e[1 + [\frac{4}{\sqrt{\pi N_e}e^2}(\frac{k_BT}{2})^{3/2}]^2] \ , \tag{1.42}$$

and with the condition 1.39

$$A_1(2) = 2log_e(\frac{4}{\sqrt{\pi e.N_e}}(\frac{k_BT}{2})^{3/2}) \ , \tag{1.43}$$

If we define d being equal to $\frac{e^2}{h\nu}$, where ν, is the radiation frequency and h is Planck's constant, 1.37 becomes

$$\nu_{01} = \frac{4k_BT}{h\nu} \ , \tag{1.44}$$

and the correction term is

$$A_1(2) = log_e[1 + (\frac{4k_BT}{h\nu})^2] \ , \tag{1.45}$$

In order to determine the numerical values of the electron collision frequencies in the upper ionosphere, we use the formulas (11) and (18). We obtain a collision frequency [48].

$$\nu_{e,+} = [34 + 8.36log_{10}\left(\frac{T^{3/2}}{\sqrt{N_e}}\right)]\frac{N_e}{T^{3/2}} \ . \tag{1.46}$$

In multi-components diffusion in gas mixture the diffusion coefficient D_j of particle j in the background gas mixture is then approximated using Blank's law [50]:

$$\frac{P_{tot}}{D_j} = \sum_{i=background} \frac{P_i}{D_{ij}} \ . \tag{1.47}$$

1.4 The plasma

Plasma is often called the 4th state of matter (99 % of the universe). A plasma is essentially a gas that consists of free positive and negative ions and electrons, gas atoms and molecules in the ground or any higher state of any form of excited species, but the overall state of the plasma is neutral. It can exist over an extremely wide range of temperature and pressure. It can be produced at low-pressure or atmospheric pressure by coupling energy to a gaseous medium by several means such as mechanical, thermal, chemical, radiant, nuclear, or by applying a voltage, or by injecting electromagnetic waves and also in many processes it may be formed during laser welding near the weld pool. In welding, the luminosity of the plasma is a very important property. The light emitted from the plasma should give us information about plasma parameters (N_e, T_e) [17, 30, 51].

1.4.1 Distribution functions for equilibrium state

The four distribution functions to describe the plasma system are:

Boltzmann distribution function:

The Boltzmann distribution gives the population ratios between the different energy of excited states i and j at the same species [52, 53]:

$$\frac{N_j}{g_j} = \frac{N_k}{g_k} \exp\left(-\frac{E_j - E_k}{k_B T_a}\right) . \tag{1.48}$$

Saha distribution function:

Saha ditribution gives the ratio of populations density of any excited state (m) belongs to some ionization stage of charge (z) with excitation energy (E_m^z) above the ionization of the previous stage $(z-1)$ with ionization energy E_i^{z-1} of the same atomic species at thermodynamic equilibrium. The following formula gives an approximate expression of this function in terms of three plasma parameters (N_e, T_e, N_o) [52–55]:

$$\frac{N_m^z}{g_m^z} = \left(\frac{N_e N_o^{z-1}}{2U_o^{z-1}}\right)\left[\frac{h^2}{2\pi m_e k_B T_e}\right]^{-3/2} \exp -\left(\frac{E_i^{z-1} + E_m^z}{k_B T_e}\right) . \tag{1.49}$$

where: E_m^z is the excitation energy of state m

Maxwell distribution function:

This function describes the velocity distribution of particles $f(v)$ in plasma [7, 52–56]:

$$f(v)dv = 4\pi v^2 \left[\frac{m_e}{2\pi k_B T_e}\right]^{3/2} \exp\left(-\frac{m_e v^2}{2k_B T_e}\right) dv . \tag{1.50}$$

Planck distribution function:

At thermodynamic equilibrium, Planck function describe the distribution of spectral light in the medium over the different wavelengths. It describing the spectral luminescence of a black body at temperature T, is given by [51–55, 57, 58]:

$$I_\lambda(T) = \frac{2hc^2}{\lambda^5}\left(\exp\left(\frac{hc}{\lambda k_B T}\right) - 1\right)^{-1} . \tag{1.51}$$

1.4.2 Equilibrium states in plasma

Plasma in Complete thermodynamic equilibrium (CTE):

The plasma are in complete thermodynamical equilibrium (CTE) when $T_e = T_a = T_i$ which enable us to use either of the four distribution functions to describe the plasma system [52, 54, 55].
Where T_e, T_a and T_i are electron temperature, atomic excitation temperature and ion temperature respectively.

Plasma in Local Thermodynamic Equilibrium (LTE):

At an electron density range (From 10^{16} to $10^{18} cm^{-3}$) and temperatures of around $1eV$, the equilibrium condition can also be applied between the different species of corpuscular nature but not for the radiation field of wave nature. In this state $T_e = T_a = T_i$ [52, 54, 55].

Plasma in Partial Local Thermodynamic Equilibrium (PLTE):

At a rather lower electron density regimes ($10^{16} > N_e > 10^{9} cm^{-3}$), the electron gas in plasma tends to divide the energy levels of the atoms into two main categories. One at the lower states where's the transition probabilities are large with respect to the collision frequency, and hence the radiative processes control the population and depopulation of such states. This is in contrast to the upper states at which the energy differences are small enough that the transition probabilities are smaller than the collision frequency. Therefore, the upper states can simply retain equilibrium with the surrounding particle species and hence they are drifting to the LTE state, while the lower ones are drifting out of the equilibrium. We call this state as partial local thermodynamic equilibrium (PLTE). The Maxwell, Boltzmann and Saha equations with equal temperatures are still applicable to the upper states only, and deviations from real (measured) values was observed at the lower lying states.

Plasma Outside TE:

Non-equilibrium plasma is a plasma which is not in thermodynamic equilibrium, because the electron temperature T_e is much hotter than the temperature of heavy species (ions and neutrals) [59]. An example of non-equilibrium plasma is the mercury-vapor gas within a fluorescent lamp, where the "electron gas" reaches a temperature of 20,000 K (19,700 $^{\circ}C$; 35,500 $^{\circ}F$) while the rest of the gas, ions and neutral atoms, stays barely above room temperature.

1.4.3 Specific Equilibrium states in plasma

Corona Equilibrium (corona state):

Corona state classified of non thermal plasma (Non equilibrium plasma); $T_e \geq T_i \approx T_g = 300....10^3 K$, and low electron density $N_e \approx 10^{16} cm^{-3}$, will lead to a very small collision frequency with respect to radiative transition probabilities even for the upper states. A characteristic feature for this state is that no two temperatures are equal for two different species [51, 52, 57].

Collisional-Radiative (CR) model:

In a collisional-radiative (CR) model, the population distribution at any point does not depend only upon plasma parameters at the point. The local population distribution is determined by balancing collisional processes of local nature and radiative processes of non-local nature.
In a CR model, atomic level populations are calculated by solving multi-level, atomic rate equations self-consistently with a radiation field.
The radiation field which induces stimulated radiative processes is computed from a radiation transport equation, which brings in non-local contributions to population distribution calculations. Due to such

non-local effects arising from radiative processes, population distributions can have a spatial gradient even when there is no gradient in plasma parameters such as temperature and density.

1.5 Some information contained in emission spectral lines

1.5.1 Spectral line radiation

Line radiation is an electron transitions from a level of principal quantum number i and energy E_i to a level j of energy E_j, the frequency ν_{ij} of this tranition is

$$h\nu_{ij} = E_i - E_j \ , \tag{1.52}$$

For allowed transitions the usual selection rules of spectroscopy have to be obeyed [60]. The total power I_λ radiated in a spectral line of frequency ν per unit source volume and per unit solid angle is:

$$I_\lambda \left(\frac{Watt}{m^3 Sr}\right) = \frac{hcA_{ji}}{4\pi\lambda_j}\frac{N_j}{g_j} \ , \tag{1.53}$$

where A_{ji} is the atomic transition probability or Einstein coefficient for spontaneous emission. For a homogeneous light source of length l and for the optically thin case, where all radiation escapes, the total emitted line intensity (SI quantity: radiance) is [61]:

$$I_{line} = I_\lambda l = \int_0^{+\infty} I(\lambda)d\lambda = \frac{hcA_{ji}l}{4\pi\lambda_j}\frac{N_j}{g_j} \ , \tag{1.54}$$

This equation can be re-written in terms of the probable number of emitting atoms per unit volume N_j. If the emitting atoms is in thermodynamic equilibrium with the surrounding (CTE, LTE or PLTE), then we can replace the term by the corresponding value given by Boltzmann equation 1.48, hence can be expressed in terms of electron temperature Te provided that is in the units of $(Watt/m^3Sr)$:

$$I_\lambda = \frac{hcA_{ji}}{4\pi\lambda_j}\left(\frac{N_j}{g_j}\right)^{Boltzmann} = \frac{hcA_{ji}}{4\pi\lambda_j}\left(\frac{N_0}{U_0}\exp\left(-\frac{E_j}{k_B T_e}\right)\right) \ , \tag{1.55}$$

Moreover, Eq. 1.53 can be further being modified "in case of using ionic lines instead " by replacing $\left(\frac{N_j}{g_j}\right)$by the corresponding value give by the Saha relation :

$$I_\lambda = \frac{hcA_{ji}}{4\pi\lambda_j}\left(\frac{N_j}{g_j}\right)^{Saha} = \frac{hcA_{ji}}{4\pi\lambda_j}\left(\frac{N_e^2}{2U_0^{z-1}}\right)\left[\frac{h^2}{2\pi m_e k_B T_e}\right]^{-3/2}\exp\left(-\frac{E_i^{z-1}+E_m^{z-1}}{k_B T_e}\right) \ . \tag{1.56}$$

In that case the spectral radiance I_λ is expressed in terms of electron density and temperature [54].

1.5.2 Line Strengths

The atomic transition probability A_{ji} and oscillator strength f_{ij} are the principal atomic quantities related to line intensities. In theoretical work, the line strength S is also widely used

$$S = S(i,j) = S(j,i) = \mid R_{ij} \mid^2 \ , \tag{1.57}$$

$$R_{ij}^2 = \frac{3\hbar}{2m_e a_0^2 \omega_{ij}}\frac{(2J_m+1)}{(2J_i+1)}f_{ij} \ . \tag{1.58}$$

where: R_{ij} involves an integration over spatial and spin coordinates of all N electrons of the atom or ion [7, 11].

1.5.3 Selection rules

Electric dipole approximation is the first term of the approach of radiative transition which induces or is emitted during transitions between different atomic energy levels [62]. The selection rules for discrete radiative transitions in electric dipole approximation are [61]:

Table 1.7 – *Selection rules for discrete transitions.*

Electric dipole E1 ("allowed")
$\Delta J = 0, \pm 1$ (except $0 \nrightarrow 0$)
$\Delta M = 0, \pm 1$ (except $0 \nrightarrow 0$ when $\Delta J = 0$)
Parity charge
One electron jumping, with $\Delta l = \pm 1$, Δn arbitrary
$\Delta S = 0$
$\Delta L = 0, \pm 1$ (except $0 \nrightarrow 0$) (except $0 \nrightarrow 0$)

1.5.4 Relationships Between A_{ji}, f_{ij}, and S_{ij}

The relationships between A_{ji}, f_{ij} , and S_{ij} for electric dipole ($E1$, or allowed) transitions; see table 1.7 are [61]:

$$A_{ji} = \frac{2\pi e^2}{m_e c \epsilon_0 \lambda^2} \frac{g_i}{g_j} f_{ij} = \frac{16\pi^3}{3h\epsilon_0 \lambda^3 g_j} S_{ij} \ , \tag{1.59}$$

For A_{ji} in s^{-1} and λ in $\mathring{A}$

$$A_{ji} = \frac{6.6702 \times 10^{15}}{\lambda^2} \frac{g_i}{g_j} f_{ij} = \frac{2.0261 \times 10^{18}}{\lambda^3 g_j} S_{ij} \ , \tag{1.60}$$

and for line strength S_{ij} and ΔE in atomic units,

$$f_{ij} = \frac{2}{3} \frac{\Delta E}{g_i} S_{ij} \ , \tag{1.61}$$

and for the lower (upper) term of a multiplet,

$$\overline{g}_{i(j)} = \sum_{J_{i(j)}} (2J_{i(j)} + 1) = (2L_{i(j)} + 1)(2S_{i(j)} + 1) \ . \tag{1.62}$$

1.6 Spectral line shapes,Widths,and Shifts

Observed spectral lines are always broadened, partly due to the finite resolution of the spectrometer and partly due to intrinsic physical causes. [61]. The broadened widths of lines have been used as diagnostic tools for plasmas. Line broadening is a function of physical parameters of the emitting particles such as pressure and temperature. Without an external influence on line broadening, a line has a finite width due to natural broadening. In most cases, however, the natural broadening is negligible, less than 10^{-4} Å. Of the various line-broadening mechanisms, Doppler broadening and Stark broadening of lines have been considered important. Doppler broadening generally prevails at high temperatures and low electron densities, while Stark broadening prevails for the opposite conditions.

1.6.1 Doppler Broadening

The motion of an emitting particle toward or away from an observer induces a wavelength shift of the emitted line, that is, a Doppler shift. Doppler broadening is the average result of Doppler shifts of line radiation produced by thermal motion of the emitting atoms or ions:

$$\frac{\Delta\lambda}{\lambda} = \pm\frac{v_s}{c} \ , \tag{1.63}$$

assuming the Maxwellian velocity distribution of particles.

$$v_{th} = \sqrt{(\frac{2k_BT}{m})} \ , \tag{1.64}$$

$$\Delta\lambda_D(\mathring{A}) = 7.17\times10^{-7}\lambda_0(\mathring{A})\sqrt{\frac{T\,(K)}{m\,(amu)}} \ . \tag{1.65}$$

1.6.2 Stark Broadening

The Stark effect in plasmas is due to collisions with fast electrons and may be slow ions, with approximate expression for neutral emitters [57]:

$$\Delta\lambda_S\,(HWHM) = 2\,[1+1.75A\,(1-0.75R)]\,\frac{w_e}{N_e^{ref}}N_e \ . \tag{1.66}$$

In this equation, w_e is the electron-impact (half) width or electron Stark broadening parameter, R is the ratio of the mean distance between ions and the Debye's length [57, 63].

Reference electron density N_e^{ref} is usually of the order of 10^{16} or 10^{17} cm^{-3}.

Theoretical models of Griem (1974), STARK-B web site:

Stark broadening parameters of non-hydrogenic neutral and ion lines is a good plasma characterization for optimum application. Two sets of theoretical data are usually used in conjunction with experimental results. Both sets of theoretical data are the result of semi-classical calculations, one performed by Griem and coworkers, (G74) [14] and the other calculated by Dimitrijević, Sahal-Brèchot and coworkers STARK-B website [13]. The results of these two semi-classical calculations differ and the overlapping data for same plasma conditions are not identical. This is the result of different approximations used for data evaluation and, in some cases, the difference is introduced by improved set of energy level data used by DSB, which were not available at the time of (G74) [14] calculations. These authors used an impact approximation for both, electrons and perturbing ions [23].

1.6.3 Van der Waals broadening

Arises from the dipole interaction of an excited atom with the induced dipole of a ground state atom. An approximate formula for the FWHM, strictly applicable to hydrogen and similar atomic structures only is [61]:

$$\Delta\lambda_{1/2}^W \simeq 3.0\times10^{-16}\lambda^2C_6^{2/5}\left(\frac{T}{\mu}\right)^{3/10}N \ , \tag{1.67}$$

where the interaction constant C_6 may be roughly estimated as follows:

$$C_6 = C_k - C_i \ , \tag{1.68}$$

with

$$C_{i(k)} = (9.8 \times 10^{10}) \alpha_d R^2_{i(k)} \ . \tag{1.69}$$

where: k, i, μ, N represent the upper and lower levels, the atom-perturber reduced mass in units of uma, the perturber density respectively. α_d is the polarisibility in cm^3 and $R^2_{i(k)}$ is transition matrix element in a_0^2

1.6.4 Natural Broadening

The natural width of a spectral line results from a radiation damping effect during a radiation emission process, the Natural broadening is negligible [61]. An atom at excited state 'm' have a life time $\tau_m$the principle of Heisenberg gives the energy interval as

$$\Delta E_m = \frac{h}{2\pi\tau_m} \ , \tag{1.70}$$

Knowing that $h\nu_{nm} = E_m - E_n$, for the transition $m \to n$, there is some dispersion of frequencies around of ν_{nm}, the natural width is [53]:

$$\Delta\nu_N = \frac{\frac{1}{\tau_m} + \frac{1}{\tau_n}}{2\pi} \ . \tag{1.71}$$

1.6.5 Spectral Line Shape and FWHM

The line shape of emitted spectral line is the functional relation between spectral radiance over a line centered at with wavelength (λ_0). This shape describes the distribution of the number of the light photons around the central emission wavelength (λ_0).

The distributions of a line shape can be a Lorentzian (Inhomogeneous distribution) or Gaussian (Homogeneous distribution) [55].

The Homogeneous Gaussian line shape can be expressed as:

$$G(\lambda) = \frac{I_0}{\sqrt{\pi}\Delta\lambda_D} \exp\left[-\left(\frac{\lambda - \lambda_0}{\Delta\lambda_D}\right)^2\right] \ , \tag{1.72}$$

Lorentzian distribution can be described by:

$$L(\lambda) = \frac{I_0}{\pi} \frac{\Delta\lambda_S}{(\lambda - \lambda_0)^2 + (0.5\Delta\lambda_S)^2} \ , \tag{1.73}$$

where we can take:

$$I_0 = A_{ji} N_0 g_j \frac{hc}{\lambda} \exp\left(-\frac{E_j}{K_B T}\right) \ , \tag{1.74}$$

The emitted spectral line contains contributions of Gaussian and Lorentzian shapes, theoretically known as the Voigt line shape, which is the integration of the convolution function between Gaussian

and Lorentzian functions. In other words, it is the multiplication of the Inverse Fourier Transform of both functions [55].

$$V(\lambda;\Delta\lambda_D;\Delta\lambda_S) = \int_{-\infty}^{+\infty} G(\lambda';\Delta\lambda_D).L(\lambda-\lambda';\Delta\lambda_S).d\lambda' \ , \tag{1.75}$$

The Voigt function is also described by the following set of equations:

$$V(\upsilon-\upsilon_0) = AK(x,y) \ , \tag{1.76}$$

where:

$$A = \frac{1}{\gamma_D}\sqrt{\frac{\ln(2)}{\pi}} \ , \tag{1.77}$$

$$K(x,y) = \frac{y}{\pi}\int_{-\infty}^{+\infty} \frac{\exp(-t^2)}{y^2+(x-t)^2}dt \ , \tag{1.78}$$

$$y = \frac{\gamma_L}{\gamma_D}\sqrt{\ln(2)} \ , \tag{1.79}$$

$$x = \frac{\nu-\nu_0}{\gamma_D}\sqrt{\ln(2)} \ , \tag{1.80}$$

where t is a variable of integration [64].

Also can be described by a very simple function [58]:

$$V(\nu) = \frac{1}{\sqrt{\pi}}\frac{1}{\Delta\nu_V}\exp\left\{-\left[\frac{\nu-\nu_0}{\Delta\nu_V}\right]^2\right\} \ , \tag{1.81}$$

where [55, 58]:

$$\Delta\lambda_V^2 \approx \Delta\lambda_D^2 + \Delta\lambda_S^2 \ . \tag{1.82}$$

1.7 Measurement of the plasma parameters using spectroscopy Technique

The spectral diagnostic technique is an effective way to study the physical parameters of plasma (N_e, T_e) the value of the electron density can be used to determine the plasma state of equilibrium, and hence the required distribution functions, while the temperature determines the strength of the variation of these functions [54, 65].

Light emitted by the plasma is very rich in information. Optical emission spectroscopy OES-technique can determine characteristic quantities of plasmas such as N_e, T_e ... etc, by analyzing the emitted light from plasma without any perturbing tools. These spectroscopic methods of optical emissions are based on the measurement of spectral lines intensity, widths (FWHM) and shifts... etc [52, 54, 55].

1.7.1 Measurement of electron density by Stark broadening

Among the OES methods proposed for electron density determination, the broadening of emission lines due to the Stark effect has been the most widely used method. Stark broadening of isolated spectral lines of non-Hydrogenic neutral atoms and ions is due mainly to electrons. As a consequence, the contribution of quasi-static ions was generally neglected and hence the Lorentzian HWHM can be approximated as [52, 54, 55].

$$\Delta\lambda_S(HWHM) = \frac{\omega_e}{N_e^{ref}}N_e \ . \tag{1.83}$$

where: ω_e is electron-impact (half) width or Stark broadening parameter wich is calculated in [7]. N_e^{ref} usually of the order of 10^{16} or 10^{17}.

1.7.2 Measurement of electron temperature using the Boltzmann plot method

In the spectral diagnosis of the welding plasma by the Boltmann plot method, there are a basic assumption is that; the welding plasma is assumed to be optically thin and in local thermal equilibrium (LTE). Taking the ratio of the spectral intensities of the two lines leads to following valid expression:

$$\frac{I_{\lambda 1}}{I_{\lambda 2}} = \left(\frac{A_{j1} g_{j1}}{\lambda_{j1}} / \frac{A_{j2} g_{j2}}{\lambda_{j2}} \right) \exp\left(\frac{E_{j2} - E_{j1}}{k_B T_e} \right) \ . \tag{1.84}$$

The Boltzmann plot with $\frac{-1}{k_B T_e}$ as the rate of slope can be obtained. In the plasma satisfying the assumption of LTE, the electron temperature T_e is approximated to the electron excitation temperature T_{exc}. In order to reduce the error in the Boltzmann plot method, The following restrictions on the chosen line pairs are summarized as [6]:

1. Be emitted from the same element.
2. Belong to the same ionization stage.
3. Wavelength difference should be very small.
4. Difference in excitation energy should be large ($\Delta E_j \geq k_B T_e$).

Chapter 2

Modeling of statistical properties of gas near weld plates

2.1 Introduction

We propose to study the statistical properties, as densities and temperatures of species, of a gas near a surface during laser welding of metal plates. The surface temperature results from the passage of a laser beam; it is taken given or calculated by other authors. The considered gas is air (O_2/N_2) under atmospheric conditions. We propose to use the equations of the fluid model. For numerical resolution we use the exponential scheme method. The considered species are electron, N_2^+, O_2^+, N_2 and O_2.

2.2 Physical hypotheses and mathematical modeling

2.2.1 Physical hypotheses

Figure 2.1 shows a simplified scheme of the gas (air: O_2/N_2) near the surface. As cited before, the considered species are electron, N_2^+ , O_2^+ , N_2 and O_2. We assume that the distribution of concentration and temperature are one-dimensional (1D); They are function of the dimensional x. We propose to use one-dimensional (1D) fluid model.

Far from the surface, we have atmospheric conditions for temperature T_{amb}, pressure P_0 and densities, the concentration rates are 20% O_2 and 80% N_2. The surface temperature is $T_{sur}(t)$. We consider that gas velocities are negligible, and the particles move by thermal velocity and diffusion phenomena related to density gradients.

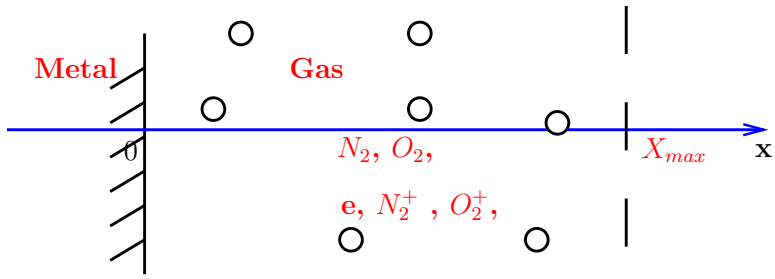

Figure 2.1 – *Simplified scheme of O_2/N_2 gas mixture near surface during Laser welding.*

Figure 2.2 shows a distribution of this temperature. The chosen temperature, for our model is calculated by Lemkeddem et al. [66].

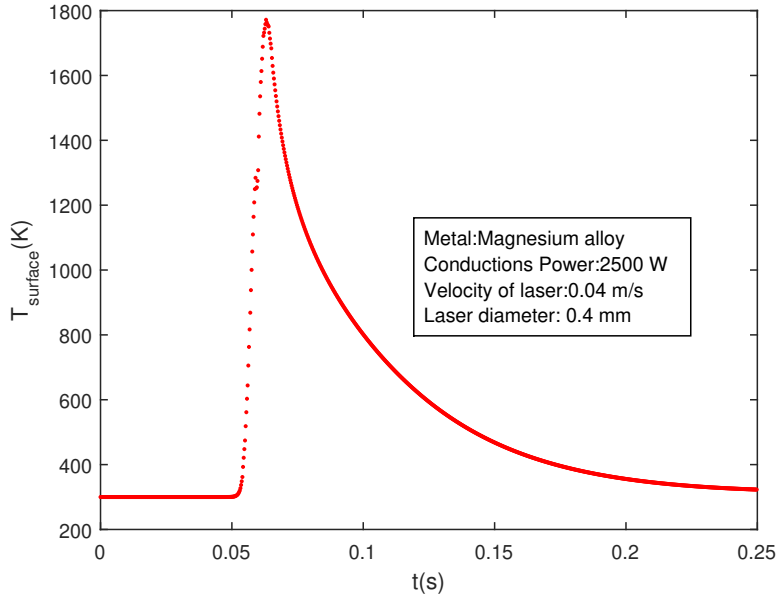

Figure 2.2 – *Calculated surface temperature by S. Lemkeddem et al. in (2018).*

For our numerical application, number of species is 5 and the number of considered chemical reactions is 6. The main reactions are shown in Table 1.1 of chapter 1. Table 1.2 of chapter 1 presents the production (or consumption) rate R of each species per unit of time and per unit of volume.

2.2.2 Basic mathematical equations

The basic mathematical equations of our model are equations of particle continuity, electron energy equation and heat equation for gas temperature. We add to this equation Poisson's equation to calculate the local electric field. As it's was shown in chapter 1, and for one-dimensional (1D) fluid model, we have the following equations. Expressions, calculation and data of transport coefficients for heat equation and transport coefficients for continuity equation were presented with detail in chapter 1.

2.3 Numerical model and boundary conditions

We use the Exponential Scheme (SG Scheme) to resolve the densities of electrons and ions and the electron energy (electron temperature). For numerical resolution of the gas temperature and neutral density equations, we use the Finite Difference Method (FDM), The two methods allow us to obtain spatio-temporal properties. As mentioned in chapter 1, these methods have been used to solve equations of fluid model and for other applications [31, 40]. The application proposed in this thesis, laser welding, is different from the fact that the regime is not stationary in time and the study of boundary conditions is very complex.

2.3.1 Exponential scheme (SG Scheme)

To resolve the nonlinear coupled equations, we use the exponential scheme (SG Scheme) [40]. The advantage of this scheme is its ability to switch between situations where either the diffusion component of the particle flux is dominant. We use one-dimensional spatial mesh and the Finite Difference Method (FDM) for numerical resolution. The continuity equation for electron and ions and the electron energy equation (electron temperature) have general form of the equation 2.1. Fluxes of particles and electron energy have general form of the equation 2.2 [40]:

$$\frac{\partial N}{\partial t} + \beta \frac{\partial J_x}{\partial x} = R \ , \tag{2.1}$$

where

$$J_x = -\mu_s N E_x - D_s \frac{\partial N}{\partial x} \ , \tag{2.2}$$

Here N is the density, J_x is the flux and β is a constant, R is the source term.
For the electron: $\beta = 1$, $J_x = J_e$, $N = N_e$, $R = R_e$.
For the ion: $\beta = 1$, $J_x = J_i$, $N = N_{ion}$, $R = R_{ion}$.
For the electron energy: $\beta = \frac{5}{3}$, $J_x = J_{e\epsilon}$, $N = \frac{3}{2} N_e k_B T_e$, $R = R_{e\epsilon}$.

For the space, we introduce a mesh of N_x nodes along x, with nodes x_i ($i = 1,\ 2,\ 3,\ ...,\ N_x$) and space step $\Delta x = x_{max}/(N_x - 1)$. For the time, we introduce discrete times $t_n = (n-1).\ \Delta t$, ($n = 1,\ 2,\ 3,\ ...$) and time step Δt. The equations 1.10 and 2.1 take the forms:

$$\Delta x \left(\frac{N_i^{n+1} - N_i^n}{\Delta t} \right) + \beta \left(J_{i+1/2}^{n+1} - J_{i-1/2}^{n+1} \right) = \Delta x R_i^n \ , \tag{2.3}$$

Electric field is calculated by direct method.

$$\left(\frac{E_{i-1}^n - E_{i+1}^n}{\Delta x} \right) = \frac{e}{\varepsilon_0} \left(N_{ion}^n - N_e^n \right) \ , \tag{2.4}$$

Flux is discretized by the SG scheme as:

$$J_{i+1/2}^{n+1} = \left(N_{i+1}^{n+1} D_{i+1}^n - N_i^{n+1} D_i^n \exp(X_1) \right) \frac{X_1}{\Delta x (1 - \exp(X_1))} \ , \tag{2.5}$$

$$J_{i-1/2}^{n+1} = \left(N_i^{n+1} D_i - N_{i-1}^{n+1} D_{i-1} \exp(X_2) \right) \frac{X_2}{\Delta x (1 - \exp(X_2))} \ , \tag{2.6}$$

where:

$$X_1 = -\frac{s\mu_{i+1/2}E_{i+1/2}}{D_{i+1/2}} = -2.e.s\frac{E_{i+1/2}}{k_B\left(T_{i+1}^n + T_i^n\right)} \ , \tag{2.7}$$

$$X_2 = -\frac{s\mu_{i-1/2}E_{i-1/2}}{D_{i-1/2}} = -2.e.s\frac{E_{i-1/2}}{k_B\left(T_i^n + T_{i-1}^n\right)} \ . \tag{2.8}$$

$s = -1$ for electrons and 1 for ions. By using the relations (2.5,2.6), we get the forms:

$$A_{i,i-1}N_{i-1}^{n+1} + A_{i,i}N_i^{n+1} + A_{i,i+1}N_{i+1}^{n+1} = B_i \ , \tag{2.9}$$

where for $i = 2, N_x - 1$:

$$\begin{cases} A_{i,i-1} & = \beta D_{i-1}^n \frac{X_2}{\Delta x(1-\exp(X_2))} \ , \\ A_{i,i} & = -\beta\left(D_i^n \exp(X_1)\frac{X_1}{\Delta x(1-\exp(X_1))} + D_i^n \frac{X_2}{\Delta x(1-\exp(X_2))}\right) - \frac{\Delta x}{\Delta t} \ , \\ A_{i,i+1} & = \beta D_{i+1}^n \frac{X_1}{\Delta x(1-\exp(X_1))} \ , \\ B_i & = \Delta x R_i^n + \Delta x \frac{N_i^n}{\Delta t} \ . \end{cases} \tag{2.10}$$

For $i = 1$ and for $i = N_x$ we use boundary conditions.

2.3.2 Finite difference method (FDM)

For the gas temperature and neutral density equations we use the finite difference method (FDM) for numerical resolution, The finite difference method (FDM) is the oldest among the discretization techniques for partial differential equations. The derivation and implementation of FDM are particularly simple on structured meshes which are topologically equivalent to a uniform Cartesian grid. The nodal value of the approximate solution at node in [67]. Finite difference approximations can be derived through the use of Taylor series expansions.

Suppose we have a function $f(x)$, which is continuous and differentiable over the range of interest. Let's also assume we know the value $f(x_0)$ and all the derivatives at $x = x_0$.

The forward Taylor-series expansion for $f(x_0 + \Delta x)$ about x_0 given by:

$$f(x_0+\Delta x) = f(x_0) + \frac{\partial f(x_0)}{\partial x}\Delta x + \frac{\partial^2 f(x_0)}{\partial^2 x}\frac{(\Delta x)^2}{2!} + \frac{\partial^3 f(x_0)}{\partial^3 x}\frac{(\Delta x)^3}{3!} \ + \frac{\partial^n f(x_0)}{\partial^n x}\frac{\Delta x^n}{n!} \ + O(\Delta x)^{(n+1)} \ , \tag{2.11}$$

We can compute the first derivative by rearranging equation 2.11:

$$\frac{\partial f(x_0)}{\partial x} = \frac{f(x_0) - f(x_0+\Delta x)}{\Delta x} - \frac{\partial^2 f(x_0)}{\partial^2 x}\frac{(\Delta x)^2}{2!} - \frac{\partial^3 f(x_0)}{\partial^3 x}\frac{(\Delta x)^3}{3!} \ , \tag{2.12}$$

This can also be written in discredited notation as:

$$\frac{\partial f(x_i)}{\partial x} = \frac{f_{i+1} - f_i}{\Delta x} + O(\Delta x)^2 \ , \tag{2.13}$$

Here $O(\Delta x)$ is called the truncation error, which means that if the distance Δx is made smaller and smaller, the (numerical approximation) error decreases as Δx. This derivative is also called first order accurate. The following equations are the Finite difference approximations of derivatives which we need it in the calcul:

$$\left|\ \frac{\partial f(x)}{\partial x}\ \right|_i = \frac{f_{i+1} - f_{i-1}}{2\Delta x} + O(\Delta x)^2 \ , \tag{2.14}$$

$$|\frac{\partial^2 f(x)}{\partial x^2}|_i = \frac{f_{i+1}-2f_i+f_{i-1}}{\Delta x^2}+O(\Delta x)^3 \ , \tag{2.15}$$

$$|\frac{\partial}{\partial x}\left(k\frac{\partial f(x)}{\partial x}\right)|_i = \frac{k_{i+1/2}\frac{f_{i+1}-f_i}{\Delta x}-k_{i-1/2}\frac{f_i-f_{i-1}}{\Delta x}}{\Delta x}+O(\Delta x)^2 \approx \frac{k_{i+1}f_{i+1}-2k_if_i+k_{i-1}f_{i-1}}{\Delta x^2} \ , \tag{2.16}$$

$$\frac{\partial f(t)}{\partial t} \approx \frac{f_i^{n+1}-f_i^n}{t^{n+1}-t^n} = \frac{f_i^{n+1}-f_i^n}{\Delta t} \ , \tag{2.17}$$

For neutral particles the mobility is set equal to zero [50]. The continuity equation for neutral density and the heat temperature have the general form:

$$\frac{\partial X}{\partial t}-\alpha\frac{\partial^2 X}{\partial x^2}=R \ , \tag{2.18}$$

where:

For neutral density: $X=N$, $\alpha=D_N$, $R=R_N$,

For gas temperature: $X=T$, $\alpha=\frac{\lambda}{\rho.C_p}$, $R=0$.

The discretization of heat and neutral concentration equations in space and time are presented as:

$$A_{i,i-1}X_{i-1}^{n+1}+A_{i,i}X_i^{n+1}+A_{i,i+1}X_{i+1}^{n+1}=B_i \ , \tag{2.19}$$

Where (for $i=2,...,N_x-1$):

$$\begin{cases} A_{i,i-1} & = -\alpha_{i-1}^n\frac{\Delta t}{\Delta x^2} \ , \\ A_{i,i} & = \left(1+2\alpha_i^n\frac{\Delta t}{\Delta x^2}\right) \ , \\ A_{i,i+1} & = -\alpha_{i+1}^n\frac{\Delta t}{\Delta x^2} \ , \\ B_i & = X_i^n+\Delta x R_i^n \ , \end{cases} \tag{2.20}$$

For $i=1$ and for $i=N_x$ we use boundary conditions.

Introducing a mesh of N nodes along x designated x_i with $i=2,3,...,N-1$ and $\Delta x=X_{max}/(N-1)$, and a mesh of nodes in time t_n with $n=1,2,...$, spacing Δt, and working forward in time, providing an implicit method for the direct determination of the unknown temperatures and concentrations at all nodes in each new time increment $n+1$. The equation 2.10 are similar to 2.20, they are a system of coupled algebraic equations with simple tri-diagonal structure;

$$\begin{pmatrix} X_1^{n+1} \\ X_2^{n+1} \\ X_3^{n+1} \\ \vdots \\ X_N^{n+1} \end{pmatrix} = \begin{pmatrix} a_{1,1} & a_{1,2} & 0 & \cdots & 0 \\ a_{2,1} & a_{2,2} & a_{2,3} & \cdots & 0 \\ 0 & a_{3,2} & a_{3,3} & \cdots & 0 \\ \vdots & \vdots & \vdots & \ddots & \vdots \\ 0 & 0 & 0 & \cdots & a_{N,N} \end{pmatrix} \begin{pmatrix} X_1^n \\ X_2^n \\ X_3^n \\ \vdots \\ X_N^n \end{pmatrix} \ , \tag{2.21}$$

Such matrix equation can be solved using standard numerical linear algebra methods like Thomas or gauss-seidel algorithm.

For computational stability, the Mesh fourier Number $F=\alpha\dfrac{\Delta t}{\Delta x^2}$ must be less than 0.5. The simplicity of the one-dimensional approach makes the calculation quick and easy in common computational software like Fortran, Matlab, Mathematica ... etc. [3]. A fortran program was developed. We chose iteratif Thomas algorithm to resolve the equations discretized [68]:

$$\begin{cases} b_1x_1+c_1x_2=d_1 \ , & \\ a_ix_{i-1}+b_ix_i+c_ix_{i+1}=d_i \ , & i=2,...imax-1 \ , \\ a_{imax}x_{imax-1}+b_{imax}x_{imax}=d_{imax} \ , & \end{cases} \tag{2.22}$$

x_1 and x_{imax} should be evaluated to find α_i and β_i as:

$$\alpha_i = \begin{cases} \frac{c_i}{b_i} \ , & i = 1 \ , \\ \frac{c_i}{b_i - a_i \alpha_{i-1}} \ , & i = 2, ...imax - 1 \ , \end{cases} \tag{2.23}$$

$$\beta_i = \begin{cases} \frac{d_i}{b_i} \ , & i = 1 \ , \\ \frac{d_i - a_i \beta_{i-1}}{b_i - a_i \alpha_{i-1}} \ , & i = 2, ...imax - 1 \ , \end{cases} \tag{2.24}$$

we find:

$$\begin{cases} x_{imax} = \beta_{imax} \ , \\ x_i = \beta_i - \alpha_i x_{i-1} \ , \quad i = imax - 1, ...1 \ . \end{cases} \tag{2.25}$$

2.3.3 Boundary and initial conditions (BIC)

In our simulation, the ambient concentration and temperature are located at $x = x_{max}$, and the surface concentration and surface temperature are located at $x = 0$.
Table 2.1 summarizes the boundary conditions and initial conditions in our calculation.

Table 2.1 – *Boundary and initial conditions.*

	limit conditions		initial conditions
symbol	at plate at $(x = 0)$	at (x_{max})	at $(t = 0)$
$N_e(cm^{-3})$	$\frac{\partial N_e(t)}{\partial x} = 0$	$N_e(0)$	10^7
$N_2^+(cm^{-3})$	$\frac{\partial N_2^+(t)}{\partial x} = 0$	$N_2^+(0)$	$0.8.10^7$
$O_2^+(cm^{-3})$	$\frac{\partial O_2^+(t)}{\partial x} = 0$	$O_2^+(0)$	$0.2.10^7$
$N_2(cm^{-3})$	$\frac{\partial N_2(t)}{\partial x} = 0$	$N_2(0)$	$0.8N_0$
$O_2(cm^{-3})$	$\frac{\partial O_2(t)}{\partial x} = 0$	$O_2(0)$	$0.2N_0$
$T_e(K)$	$\frac{\partial T_e(t)}{\partial x} = 0$	$T_e(0)$	300.
$T_g(K)$	$T(t)$	$T(0)$	300.
$E(V/cm)$	/	0	/

2.3.4 Diagram

The flow-diagram of steps in the mathematical modeling is shown in Figure. 2.3. We have to note that, X_f=(T_g, or T_e, or N_e, or N_2, or O_2, or N_2^+, or O_2^+). We have a loop on iterative calculation ($igs = igs + 1$) and another loop on time ($it = it + 1$).

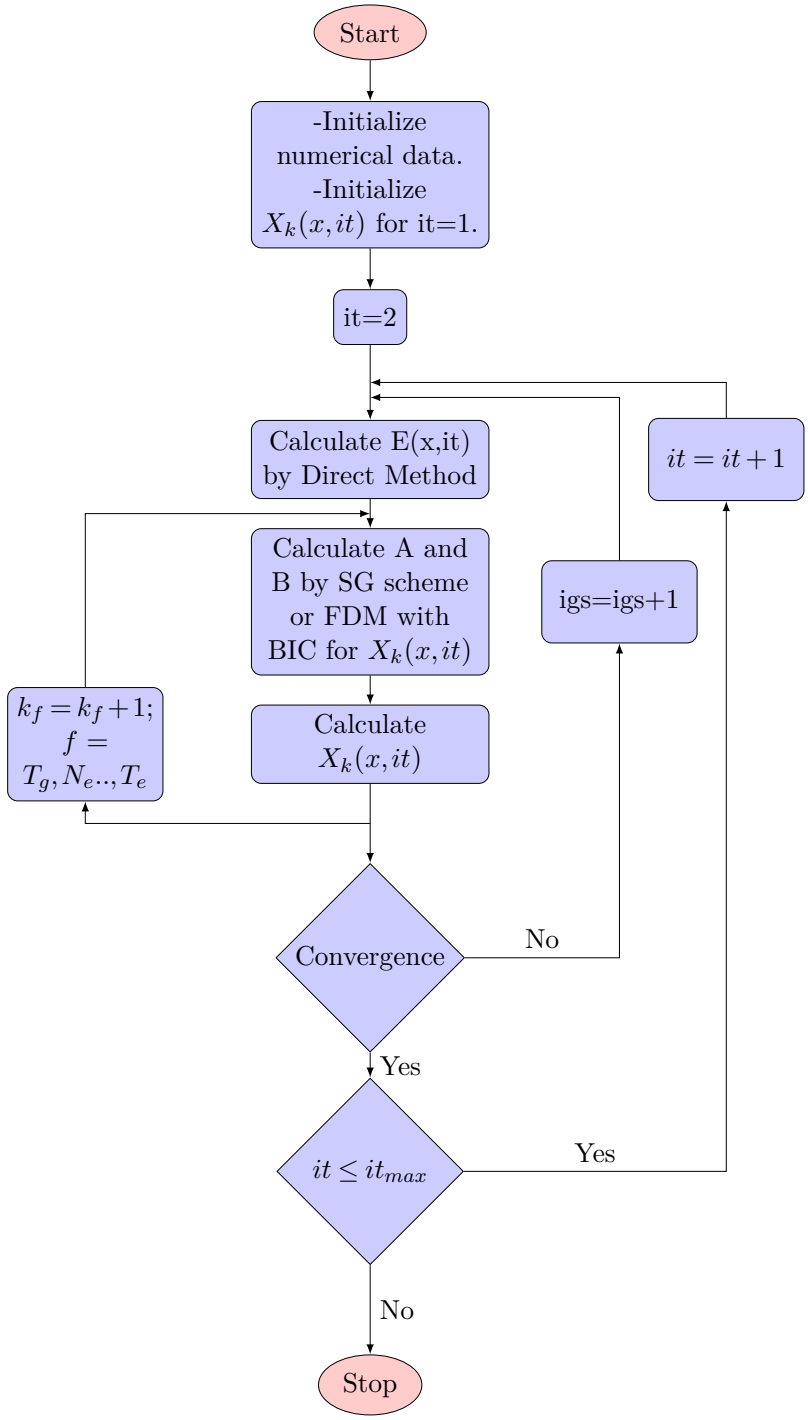

Figure 2.3 – *Flow-diagram of the modeling of statistical properties*

Figure 2.3 shows presentation of the model and the numerical procedure based on the exponential scheme method. The studied species are N_2, O_2, N_2^+, O_2^+ and electrons and temperatures.

Chapter 3

Electronic Stark broadening using an analytical model based on limits of impact parameter

3.1 Introduction

Many problems have been solved by the very active experimental and theoretical research on Stark broadening that began in the 1950's [14]. Stark broadening of spectral lines by plasmas has been used as an important plasma diagnostic tool for a number of years. Many of this work was concerned the Stark broadening of hydrogen lines. Because of the large linear Stark effect, these studies were useful for diagnostic in plasmas. However, it is not always convenient to seed a plasma with hydrogen, and sometimes it is not possible to do so. Further, because of the large Stark effect, hydrogen lines may not be useful for diagnostic purposes; since they become so broad at high electron densities that it is difficult to determine a line shape because of interference with neighboring lines. Therefore, there has been interest in the Stark broadening of non-hydrogenic lines of neutrals and ions [69].

In general, Stark broadening tends to be important for lines of allowed electric dipole transitions. When Stark widths are large, collision induced transition rates are large as well, and relative populations of neighboring levels are not negligible. Intensities of so-called forbidden lines become not negligible (because of the microfield of ions). In an electric field, a linear Stark effect exists for hydrogen; for all other atoms the interaction is quadratic [28]. In plasmas, the Stark effect is due to interaction of the emitting atoms (or ions) with microelectric fields produced by electrons and ions. Generally, this interaction leads to spectral line shift and broadening (width) of the upper emitting state [57].

Stark widths and shifts are normally computed from two extreme approximations, in general, the impact theory and the quasi-static theory. Electron collisions effect can be presented by electronic

collision operator [14, 70]. The basic concept of the impact theory is that a wave train of emitted light is perturbed by instantaneous impacts of charged particles (usually electrons) and cut completely into a number of smaller independent wave trains [57]. It takes into account nonadiabatic effects due to the electron collisions [71]. The line profile is closely approximated by a Lorentz profile. The impact theory is usually used to treat collisions with electrons. The quasi-static theory considers the emitting particles to be under the continuous influence of perturbers during the whole emission process. Perturbing particles are assumed to move so slowly during an emission that the perturbing field is assumed to be quasi-static. The quasi-static theory is used to treat the heavy, slowly moving ions. Comparison between experiments and theories indicates that both ions and electrons should be considered in computing Stark widths [57]. The experimentally observed line shapes are usually the result of several broadening factors from which the Stark profile component has to be isolated and retrieved. While the experiments reporting plasma broadening data are usually designed so as to have Stark broadening as the dominant cause of the width, the conditions can rarely be made so ideal that all broadening factors become insignificant. When line shapes are used for plasma diagnostic purposes, in most of the cases, one cannot change plasma conditions so the contribution of other broadening mechanisms has to be carefully estimated and, if necessary, measured widths corrected. Stark broadening is of particular interest for a large number of problems which concern laboratory plasma spectroscopy and astrophysics as well.

In this chapter, we describe simple method for calculation the contribution of electrons to the broadening using the impact theory which takes into account nonadiabatic effects due to electron collisions [71]. We neglect the contribution of ion to the broadening to the widths of isolated lines; ion contribution is usually less than 20% for many spectral lines [72]. The corresponding profiles are, therefore, of dispersion (Lorentz-Weisskopf) type. Because of the long-range nature of the (dipole-monopole) interaction between emitting atoms and perturbing electrons, perturbation theory can be used to calculate the dominant, terms in widths and shifts of these dispersion profiles. We apply this theory to the isolated neutral lines of magnesium. The isolated lines are the lines whose half-width is much smaller than the separation between the perturbed level α and the next interacting level α' that is to say $\lambda_{width} << \lambda_{\alpha\alpha'}$ ($\lambda_{\alpha\alpha'}$ is the separation between levels α and α' whereas λ_{width} is the half width of the spectral line). Practically all the broadening is caused by interactions between the upper state of the line in question and its neighbors, and lower state interactions can be neglected [72].

3.2 Theoretical Implementation

To calculate the electronic broadening using electronic collision operator in impact approximation, we have to calculate the contributions of all transitions that respect the selection rules in electrical dipole approximation in particular $\Delta J = 0, \pm 1$. But, it is sufficient to keep a few neighbor states; we can take less than five states [73]. In the calculation of the latter, we need the minimum value of the impact parameter $\rho_{\min}$ defined by the criteria of the unitarity of S-matrix that gives [14]:

$$(\rho_{\min})^2 = \frac{2e^4}{3\hbar^2 V^2} a_0^2 \sum_{\alpha'} R^2_{\alpha\alpha'} \sqrt{A^2(z^{\alpha\alpha'}_{\min}) + B^2(z^{\alpha\alpha'}_{\min})}\ , \tag{3.1}$$

where $R^2_{\alpha\alpha'}$ is the dimensionless matrix element of the position operator of the bounded electron, a_0 is the Bohr radius and:

$$z^{\alpha\alpha'}_{\min} = \omega_{\alpha\alpha'}\frac{\rho_{\min}}{V} \equiv \omega_{\alpha\alpha'}t_{\min} \ , \tag{3.2}$$

For a velocity V of free electron and a angular frequency separation $\omega_{\alpha\alpha'}$ between the sublevels α and α', we have:

$$t^2_{\min} = \frac{2}{3}\left(\frac{\hbar}{m_e V^2}\right)^2 \sum_{\alpha'} R^2_{\alpha\alpha'} \cdot\sqrt{A^2(\omega_{\alpha\alpha'}t_{\min}) + B^2(\omega_{\alpha\alpha'}t_{\min})} \ , \tag{3.3}$$

such that [14]:

$$A(z) = z^2\left[K_0^2(z) + K_1^2(z)\right] \ \equiv z^2 a(z) \ , \tag{3.4}$$

$$B(z) = \pi z^2\left[K_0(z)I_0(z) - K_1(z)I_1(z)\right] \equiv \pi z^2 b(z) \ , \tag{3.5}$$

Using these definitions, and the formula (3.15) of the paper [74] between the oscillator strength $f_{\alpha\alpha'}$ and $R_{\alpha\alpha'}$ (J_m refers to the value of the angular momentum of the lower state among the sublevels α and α'):

$$R^2_{\alpha\alpha'} = \frac{3\hbar}{2m_e a_0^2 \omega_{\alpha\alpha'}}\frac{(2J_m+1)}{(2J_\alpha+1)} f_{\alpha\alpha'} \ , \tag{3.6}$$

we obtain, the following relation between the minimum of the impact parameter and the velocity of the free colliding electron:

$$\left(\frac{m_e}{\hbar}\right)^3 V^4 = \sum_{\alpha'} F_{\alpha,\alpha'}\omega_{\alpha\alpha'} \cdot \sqrt{a^2(\omega_{\alpha\alpha'}t_{\min}) + \pi^2 b^2(\omega_{\alpha\alpha'}t_{\min})} \ , \tag{3.7}$$

where we have, for lightening the subsequent equations, defined:

$$F_{\alpha,\alpha'} = \frac{(2J_m+1)}{(2J_\alpha+1)}\frac{f_{\alpha\alpha'}}{a_0^2} \ , \tag{3.8}$$

To find the minimum of the impact parameter $\rho_{\min}$, we have to solve the last equation to get $t_{\min}$ as function of V then we obtain $\rho_{\min} = Vt_{\min}$. To reach this goul, we have studied deeply the function $\sqrt{a^2(z) + \pi^2 b^2(z)}$; we conclude that the function has two different behaviors with respect $z < 1$ or $z > 1$. Then we define a critical velocity V_c, by putting $\omega_{\alpha\alpha'}t_{\min} = 1$ in the equation (3.7) as:

$$V_c = 0.94907\left(\frac{\hbar}{m_e}\right)^{3/4}\left(\sum_{\alpha'} F_{\alpha,\alpha'}\omega_{\alpha\alpha'}\right)^{1/4} \ , \tag{3.9}$$

By defining the reduced critical velocity v_c (with dimensionless unit):

$$v_c = \sqrt{\frac{m_e}{2k_B T_e}} V_c \ , \tag{3.10}$$

we obtain:

$$v_c = 0.94907\left(\sum_{\alpha'} a_0^2 F_{\alpha\alpha'}\frac{E_H}{k_B T_e}\frac{\hbar\omega_{\alpha\alpha'}}{2k_B T_e}\right)^{1/4} \ , \tag{3.11}$$

where $E_H = e^2/(2a_0)$ is the fundamental Bohr energy. Going back now to solve the equation (3.7): the square root can be replaced, with a good approximation, by $1/(\omega_{\alpha\alpha'}t_{\min})^2$ for $\omega_{\alpha\alpha'}t_{\min} < 1$ and by $(4/5)/(\omega_{\alpha\alpha'}t_{\min})^3$ for $\omega_{\alpha\alpha'}t_{\min} > 1$. In the case of $\omega_{\alpha\alpha'}t_{\min} < 1$, where is $V < V_c$, we have:

$$t_{\min}^2 = \frac{1}{V^4}\left(\frac{\hbar}{m_e}\right)^3 \sum_{\alpha'} \frac{F_{\alpha\alpha'}}{\omega_{\alpha\alpha'}} \ , \tag{3.12}$$

or, by taking the square root:

$$t_{\min} = \frac{1}{V^2}(\frac{\hbar}{m_e})^{3/2}(\sum_{\alpha'} \frac{F_{\alpha\alpha'}}{\omega_{\alpha\alpha'}})^{1/2} \ , \tag{3.13}$$

and the minimum of impact parameter $\rho_{\min}^{(1)} = Vt_{min}$ for $V < V_c$:

$$\rho_{\min}^{(1)} = \frac{1}{V}(\frac{\hbar}{m_e})^{3/2}(\sum_{\alpha'} \frac{F_{\alpha\alpha'}}{\omega_{\alpha\alpha'}})^{1/2} \ , \tag{3.14}$$

In the case of $\omega_{\alpha\alpha'}t_{\min} > 1$, where is $V > V_c$, the equation (3.7) takes the following formula:

$$\left(\frac{m_e}{\hbar}\right)^3 V^4 = \sum_{\alpha'} F_{\alpha,\alpha'}\omega_{\alpha\alpha'} \frac{(4/5)}{(\omega_{\alpha\alpha'}t_{\min})^3} \ , \tag{3.15}$$

that is to say:

$$t_{\min} = \left[\frac{4}{5V^4}(\frac{\hbar}{m_e})^3 \sum_{\alpha'} \frac{F_{\alpha\alpha'}}{\omega_{\alpha\alpha'}^2}\right]^{1/3} \ , \tag{3.16}$$

and the minimum of impact parameter $\rho_{\min}^{(2)}$, for the case $V > V_c$, is given by:

$$\rho_{\min}^{(2)} = \frac{\left(\frac{\hbar}{m_e}\right)}{V^{1/3}}\left(\frac{4}{5}\sum_{\alpha'} \frac{F_{\alpha\alpha'}}{\omega_{\alpha\alpha'}^2}\right)^{1/3} \ . \tag{3.17}$$

Once all necessary parameters are ready, we can compute the contribution of strong collisions (for impact parameter less than $\rho_{\min}$) and of weak collisions (for impact parameter great than $\rho_{\min}$).

3.3 Strong Collision Contribution

To compute the strong collisions contribution to collision operator, we use Maxwell's distribution of the velocities $f(V)$:

$$f(V)d^3V = 4\pi V^2\left(\frac{m_e}{2\pi k_B T_e}\right)^{3/2} \exp(-\frac{m_e V^2}{2k_B T_e})dV \ , \tag{3.18}$$

so that, we have [71]:

$$\phi_\alpha^{strong} = -\pi N_e \int_0^\infty V\rho_{\min}^2 f(V)d^3V \tag{3.19}$$

$$= -4\pi^2 N_e\left(\frac{m_e}{2\pi k_B T_e}\right)^{3/2} \int_0^\infty V^3\rho_{\min}^2 \exp(-\frac{m_e V^2}{2k_B T_e})dV \ , \tag{3.20}$$

By expliciting the integral, in two regions with respect the expressions of the impact parameter given by (3.14) and (3.17), we find:

$$\phi_\alpha^{strong} = \phi_\alpha^{strong1} + \phi_\alpha^{strong2} \ , \tag{3.21}$$

such that:

$$\phi_\alpha^{strong1} = -4\pi^2 N_e \left(\frac{m_e}{2\pi k_B T_e}\right)^{3/2} \int_0^{V_c} \left(\rho_{\min}^{(1)}\right)^2 V^3 \exp(-\frac{m_e V^2}{2k_B T_e}) dV \ ,$$

and

$$\phi_\alpha^{strong2} = -4\pi^2 N_e \left(\frac{m_e}{2\pi k_B T_e}\right)^{3/2} \int_{V_c}^{\infty} \left(\rho_{\min}^{(2)}\right)^2 V^3 \exp(-\frac{m_e V^2}{2k_B T_e}) dV \ ,$$

or more explicitly:

$$\phi_\alpha^{strong1} = -4\pi^2 N_e \left(\frac{\hbar}{m_e}\right)^3 \left(\frac{m_e}{2\pi k_B T_e}\right)^{3/2} \left(\sum_{\alpha'} \frac{F_{\alpha\alpha'}}{\omega_{\alpha\alpha'}}\right) \int_0^{V_c} V \exp(-\frac{m_e V^2}{2k_B T_e}) dV \ , \tag{3.22}$$

and

$$\phi_\alpha^{strong2} = -4\pi^2 N_e (\frac{m_e}{2\pi k_B T_e})^{3/2} (\frac{\hbar}{m_e})^2 \left(\frac{4}{5} \sum_{\alpha'} \frac{F_{\alpha\alpha'}}{\omega_{\alpha\alpha'}^2}\right)^{2/3} \int_{V_c}^{\infty} V^{7/3} \exp(-\frac{m_e V^2}{2k_B T_e}) dV \ , \tag{3.23}$$

When we perform the integrals in formulas (3.22-3.23), we find:

$$\phi_\alpha^{strong1} = -2\sqrt{\pi} N_e \left(\frac{\hbar}{m_e}\right)^3 \left(\frac{m_e}{2k_B T_e}\right)^{1/2} \left(\sum_{\alpha'} \frac{F_{\alpha\alpha'}}{\omega_{\alpha\alpha'}}\right) \left(1 - \exp(-\frac{m_e V_c^2}{2k_B T_e})\right) \ , \tag{3.24}$$

$$\phi_\alpha^{strong2} = -4\pi^2 N_e \left(\frac{m_e}{2\pi k_B T_e}\right)^{3/2} \left(\frac{\hbar}{m_e}\right)^2 \left(\frac{4}{5} \sum_{\alpha'} \frac{F_{\alpha\alpha'}}{\omega_{\alpha\alpha'}^2}\right)^{2/3} F(q, V_c) \ , \tag{3.25}$$

where:

$$\begin{aligned} F(q, V_c) &= \int_{V_c}^{\infty} V^{7/3} \exp(-\frac{m_e V^2}{2k_B T_e}) dV \\ &= \frac{k_B T_e}{m_e} V_c^{4/3} \exp(-\epsilon_c) + \frac{1}{3} \left(\frac{2k_B T_e}{m_e}\right)^{5/3} \Gamma(\frac{2}{3}, \epsilon_c) \ . \end{aligned} \tag{3.26}$$

and $\Gamma(a, x)$ is a non-complete gamma Euler function and $\epsilon_c = (m_e V_c^2)/(2k_B T_e)$. Formulas (3.24-3.25) are the key formula to get the contribution of strong collisions to the broadening of the level α by electron collisions.

3.4 Weak Collision Contribution

Recall that the minimal impact parameter $\rho_{\min}$ has two expressions $\rho_{\min}^{(1)}$ or $\rho_{\min}^{(2)}$ with respect to the colliding electron if it has a velocity less or greater than the critical velocity V_c. We take the maximum of the impact parameter that correspond to the Debye length [56, 75], and we have:

$$z_{min}^{(1,2)} = \frac{\omega_{\alpha\alpha'}}{V} \rho_{\min}^{(1,2)}, \quad z_{\max} = \frac{\omega_{\alpha\alpha'}}{V} \lambda_D \ , \tag{3.27}$$

from which, we can write, the weak collisions contribution to the collision operator as Griem (1962) [71] in the hydrogen-like approximation, as:

$$\phi_\alpha^{weak} = \frac{16\sqrt{\pi}}{3} N_e \sqrt{\frac{m_e}{2k_B T_e}} \left(\frac{\hbar}{m_e}\right)^2 \sum_{\sigma\alpha'} r_\sigma^{\alpha,\alpha'} r_\sigma^{\alpha',\alpha} \int_0^\infty v dv \exp(-v^2) \int z dz \left[(K_0(z))^2 + (K_1(z))^2 \right] , \tag{3.28}$$

The integration over z is between z_{min} and z_{max} defined by (3.27). By separating the integral over two regions ($v < v_c$ and $v > v_c$: here v is a dimensionless velocity $v = V\sqrt{m/2k_BT_e}$ and v_c is given by (3.11) and doing the sum over the components of the position vector, we find

$$\phi_\alpha^{weak} = \frac{16\sqrt{\pi}}{3} N_e \sqrt{\frac{m_e}{2k_B T_e}} (\frac{\hbar}{m_e})^2 \sum_{\alpha'} R^2_{\alpha\alpha'} \int_0^{v_c} v dv \exp(-v^2) \int_{z_{min}^{(1)}}^{z_{max}} z dz a(z) + \int_{v_c}^\infty v dv \exp(-v^2) \int_{z_{min}^{(2)}}^{z_{max}} z dz a(z)] , \tag{3.29}$$

where $a(z)$ is defined by the formula (3.4). By using (3.6) and (3.8) and after integrating over z, we obtain:

$$\phi_\alpha^{weak} = \frac{3}{2} Q \sum_{\alpha'} \frac{F_{\alpha\alpha'}}{\omega_{\alpha\alpha'}} [\int_0^{v_c} v dv \exp(-v^2) Bes1(v,\omega_{\alpha\alpha'}) + \int_{v_c}^\infty v dv \exp(-v^2) Bes2(v,\omega_{\alpha\alpha'})] , \tag{3.30}$$

where Q, $Bes1(v,\omega_{\alpha\alpha'})$ and $Bes2(v,\omega_{\alpha\alpha'})$ are given consecutively by:

$$Q = \frac{16\sqrt{\pi}}{3} N_e \sqrt{\frac{m_e}{2k_B T_e}} \left(\frac{\hbar}{m_e}\right)^3 , \tag{3.31}$$

$$Bes1 = Bes(z_{max}) - Bes(z_{min}^{(1)}(v,\omega_{\alpha\alpha'})) , \tag{3.32}$$

$$Bes2 = Bes(z_{max}) - Bes(z_{min}^{(2)}(v,\omega_{\alpha\alpha'})) , \tag{3.33}$$

and $Bes(z) = zK_0(z)K_1(z)$. If we neglect the terms coming from $z_{\max}$(because $\lambda_D >> \rho_{\min}$ and the fact that the function $xK_0(x)K_1(x)$ is strongly decreasing function), we find $\phi_\alpha^{weak} = \phi_\alpha^{weak1} + \phi_\alpha^{weak2}$ such that:

$$\phi_\alpha^{weak1} \simeq -Q \sum_{\alpha'} \frac{3}{2} \frac{F_{\alpha\alpha'}}{\omega_{\alpha\alpha'}} \int_0^{v_c} v dv \exp(-v^2) Bes(z_{min}^{(1)}(v,\omega_{\alpha\alpha'})) , \tag{3.34}$$

and:

$$\phi_\alpha^{weak2} \simeq -Q \sum_{\alpha'} \frac{3}{2} \frac{F_{\alpha\alpha'}}{\omega_{\alpha\alpha'}} \int_{v_c}^\infty v dv \exp(-v^2) Bes(z_{min}^{(2)}(v,\omega_{\alpha\alpha'})). \tag{3.35}$$

To compute the formulas (3.34) and (3.35), we have to explict the two quantities $z_{min}^{(1)}(v,\omega_{\alpha\alpha'})$ and $z_{min}^{(2)}(v,\omega_{\alpha\alpha'})$. The first quantity is based on formula (3.14) and the second on the formula (3.17). In

fact we have:

$$\begin{aligned} z_{min}^{(1)}(v,\omega_{\alpha\alpha'}) &= \frac{\omega_{\alpha\alpha'}}{V}\rho_{\min}^{(1)} \\ &= \frac{1}{v^2}\frac{m_e\omega_{\alpha\alpha'}}{2k_BT_e}\left(\frac{\hbar}{m_e}\right)^{3/2}\left(\sum_{\alpha'}\frac{F_{\alpha\alpha'}}{\omega_{\alpha\alpha'}}\right)^{1/2}, \\ &= \frac{\sqrt{2}}{v^2}\frac{\Delta E_{\alpha\alpha'}}{2k_BT_e}\left(\sum_{\alpha'}a_0^2F_{\alpha\alpha'}\frac{E_H}{\Delta E_{\alpha\alpha'}}\right)^{1/2} = \frac{P_{\alpha\alpha'}}{v^2}\ . \end{aligned} \tag{3.36}$$

where we have defined:

$$P_{\alpha\alpha'} = \sqrt{2}\frac{\Delta E_{\alpha\alpha'}}{2k_BT_e}\left(\sum_{\alpha'}a_0^2F_{\alpha\alpha'}\frac{E_H}{\Delta E_{\alpha\alpha'}}\right)^{1/2},$$

and:

$$\begin{aligned} z_{min}^{(2)}(v,\omega_{\alpha\alpha'}) &= \frac{\omega_{\alpha\alpha'}}{V}\rho_{\min}^{(2)} \\ &= \frac{\omega_{\alpha\alpha'}}{\left(\frac{2k_BT_e}{m_e}\right)^{2/3}}\frac{\left(\frac{\hbar}{m_e}\right)}{v^{4/3}}\left(\frac{4}{5}\sum_{\alpha'}\frac{F_{\alpha\alpha'}}{\omega_{\alpha\alpha'}^2}\right)^{1/3}, \end{aligned} \tag{3.37}$$

or equivalently:

$$\begin{aligned} z_{min}^{(2)} &= \frac{1}{v^{4/3}}\left(\frac{\Delta E_{\alpha\alpha'}}{2k_BT_e}\right)\left(\frac{\hbar}{e^2}\right)^{2/3}\left(\frac{2k_BT_e}{m_e}\right)^{1/3} \\ &\quad\left(\frac{16}{5}\sum_{\alpha'}a_0^2F_{\alpha\alpha'}\left(\frac{E_H}{\Delta E_{\alpha\alpha'}}\right)^2\right)^{1/3} \\ &= \frac{1}{v^{4/3}}\left(\frac{\Delta E_{\alpha\alpha'}}{2k_BT_e}\right)\left(\frac{k_BT_e}{E_H}\right)^{1/3} \\ \cdot\left(\frac{16}{5}\sum_{\alpha'}a_0^2F_{\alpha\alpha'}\left(\frac{E_H}{\Delta E_{\alpha\alpha'}}\right)^2\right)^{1/3} &\equiv \frac{\Lambda_{\alpha\alpha'}}{v^{4/3}}\ . \end{aligned} \tag{3.38}$$

where:

$$\begin{aligned} \Lambda_{\alpha\alpha'} &= \left(\frac{\Delta E_{\alpha\alpha'}}{2k_BT_e}\right)\left(\frac{k_BT_e}{E_H}\right)^{1/3} \\ &\quad\cdot\left(\frac{16}{5}\sum_{\alpha'}a_0^2F_{\alpha\alpha'}\left(\frac{E_H}{\Delta E_{\alpha\alpha'}}\right)^2\right)^{1/3}\ . \end{aligned} \tag{3.39}$$

To obtain (3.36) and (3.38), we have used the fact that $E_H = e^2/2a_0$ and $a_0 = \hbar/m_ee^2$

3.5 Full Electronic Width and Stark Broadening

3.5.1 Full electronic width

The full electronic width (strong and weak) is then the sum of (3.24) and (3.25) for strong collision and (3.34 -3.35) for weak collision. Formula (3.30) can be simplified if the following considerations are satisfied: if the reduced critical velocity (3.11) is small ($v_c << 1$) and if the first integral in (3.30) is

canceled, such that:

$$\phi_\alpha^{weak} \simeq -\frac{16\sqrt{\pi}}{3} N_e \sqrt{\frac{m_e}{2k_B T_e}} \left(\frac{\hbar}{m_e}\right)^3 \sum_{\alpha'} \frac{3}{2} \frac{F_{\alpha\alpha'}}{\omega_{\alpha\alpha'}} \cdot \int_0^\infty v dv \exp(-v^2) z_{min}^{(2)} K_0(z_{min}^{(2)}) K_1(z_{min}^{(2)}) \ , \tag{3.40}$$

By replacing $z_{min}^{(2)}$ by its expression given by (3.38), the formula (3.40) transforms to:

$$\phi_\alpha^{weak} \simeq -Q \sum_{\alpha'} \frac{3}{2} \frac{F_{\alpha\alpha'} \Lambda_{\alpha\alpha'}}{\omega_{\alpha\alpha'}} \int_0^\infty \frac{dv}{v^{1/3}} \exp(-v^2) K_0(\frac{\Lambda_{\alpha\alpha'}}{v^{4/3}}) K_1(\frac{\Lambda_{\alpha\alpha'}}{v^{4/3}}) \ , \tag{3.41}$$

The change $x = v^{2/3}$ gives $\frac{3}{2}dx = \frac{dv}{v^{1/3}}$ and:

$$\phi_\alpha^{weak} \simeq -\frac{9}{4} Q \sum_{\alpha'} \frac{F_{\alpha\alpha'} \Lambda_{\alpha\alpha'}}{\omega_{\alpha\alpha'}} \int_0^\infty dx \exp(-x^3) K_0(\frac{\Lambda_{\alpha\alpha'}}{x^2}) K_1(\frac{\Lambda_{\alpha\alpha'}}{x^2}) \ , \tag{3.42}$$

The last integral can be expressed with the help of Meijer's G-functions $\Phi(\Lambda_{\alpha\alpha'})$, [56, 76]:

$$\phi_\alpha^{weak} \simeq -\frac{9}{4} Q \sum_{\alpha'} \frac{F_{\alpha\alpha'} \Lambda_{\alpha\alpha'}}{\omega_{\alpha\alpha'}} \Phi(\Lambda_{\alpha\alpha'}) \ . \tag{3.43}$$

such that $\Lambda_{\alpha\alpha'}$ is given by (3.39). The result (3.43) is new and is useful when the critical velocity ($v_c << 1$). In this case, where $v_c << 1$, the strong collision contribution is given by the formula (3.25). We can then assert that when $v_c << 1$, the contribution of the collision operator is given by the sum of the formulas (3.25) and (3.43). Viewing the formulas (3.10-3.11), this case occurs at high temperatures (5000-50000 K) and for high ionization energy elements in stellar plasmas.

3.5.2 Stark broadening

The full Stark width $\Delta\lambda_{Stark}$ in $(\mathring{A})$ (ionic and electronic) is given by [14]:

$$\Delta\lambda_{Stark} = 2\phi(1 + 1.75A(1 - 0.75R)) \ , \tag{3.44}$$

Where ϕ is given by:

$$\phi = \phi_{strong} + \phi_{weak} \ , \tag{3.45}$$

and:

$$A = \frac{4\pi N_e}{3} (\frac{1}{3\phi} (\frac{\hbar}{m_e})^2 \sum_{\alpha'} \frac{|\langle\alpha|\overrightarrow{r}|\alpha'\rangle|^2}{\omega_{\alpha,\alpha'}})^{3/4} = \frac{1}{\phi^{3/4}} \frac{4\pi N_e}{3} (\frac{1}{3} (\frac{\hbar}{m_e})^2 \sum_{\alpha'} \frac{|\langle\alpha|\overrightarrow{r}|\alpha'\rangle|^2}{\omega_{\alpha,\alpha'}})^{3/4} \ , \tag{3.46}$$

and:

$$R(N_e, T_e) = (36\pi N_e)^{1/6} \sqrt{\frac{e^2}{k_B T_e}} . \tag{3.47}$$

In this equation, ϕ is the electron-impact (half) width or Stark broadening parameter, N_e is the electron density. A is the ion broadening parameter, which is a measure of the relative importance of the collisions with ions in the broadening. Parameters ϕ and A are measured or calculated; they are weak functions of temperature. R is the ratio of the mean distance between ions and the Debye's length [57, 63]. The first term in equation (3.44) of $\Delta\lambda_{Stark}$ is caused by electron collisions and it is very sensitive to the electron temperature. The second term in this equation that describe the contribution of ion broadening are very small and negligible [77]. This equation is valid only in the range $A \leq 0.5,\ R \leq 0.8$. Also, this equation is valid for neutral emitters. For singly ionized emitters, the term 0.75R should be replaced by about 1.2R [63].

Focus on the electronic broadening of spectral lines which is estimated via a collision operator. She distinguished between strong and weak collisions due to electrons which is the lighter particles in the plasma.

Chapter 4

Temperatures and densities of particles of gas near weld plates

4.1 Introduction

In this chapter, we will use the modeling proposed in Chapter 2 to calculate the temporal and spatial distributions of densities and temperatures near the surface of a metal during laser welding. The variation of the surface temperature of a magnesium metal is that calculated by S. Lemkeddem et al. [66]. For the O_2/N_2 gas mixture, the different selected species are O_2, N_2, O_2^+, N_2^+ and the electrons. Solutions of analytical forms of the distributions are requested for possible exploitation of the parameters of plasma and welding.

4.2 Temporal and spatial distribution of electron density

We chose a specific time indexes characteristic times for surface temperature during laser welding. Let T_0 be the initial temperature and T_{max} the maximum temperature at the weld bead during welding; and let T_{moy} be the temperature corresponding to $T_{moy} = \frac{T_{max}}{2}$ and T_{min} the minimum temperature after the passage of the laser beam. T_{min} is slightly greater than T_0. Let t_0, t_1, t_2, t_3 and t_4 be the characteristic times for surface temperature corresponding respectively to temperatures T_0, $T_1 = T_{moy}$ (before T_{max}), $T_2 = T_{max}$, $T_3 = T_{moy}$ (after T_{max}) and T_{min} (see figure 4.1). We have chosen to calculate the temperatures and densities near the surface for a maximum distance $X_{max} = 3$ cm. To see the effect of dynamics as a function of time and space, we have chosen a few significant positions x_0, x_1, x_2, x_3, x_4, x_5 and x_6. The temperature and density profiles are different for these positions. Indeed, X_0 and X_1 are practically the surface; for X_5 and X_6, these are the conditions for the ambient environment.

Numerical values of characteristic times and significant positions are presented in Table 4.1. Figure 4.1 shows the characteristic times for surface temperature during laser welding.

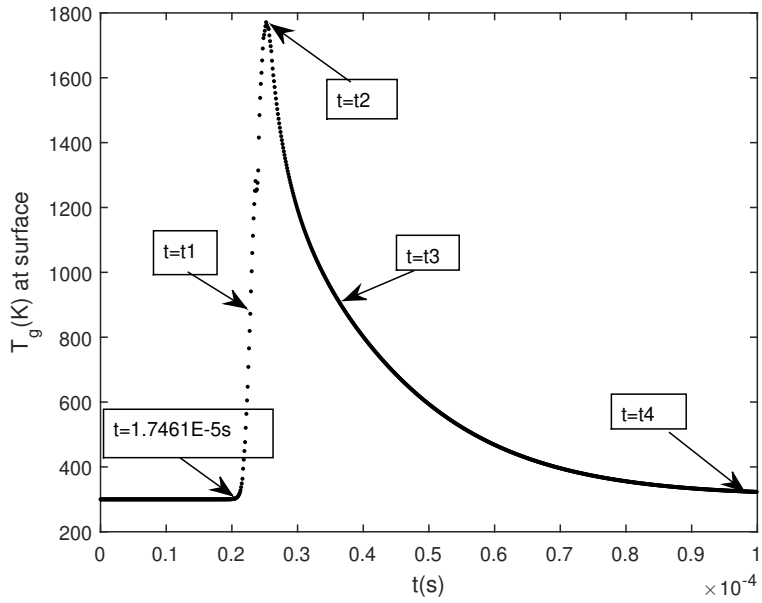

Figure 4.1 – *Characteristic times for surface temperature.*

Table 4.1 presents the characteristic times for surface temperature during laser welding and significant positions chosen to see the effect of dynamics as a function of time and space.

Table 4.1 – *Values of characteristic times and significant positions.*

Characteristic times	value in 10^{-5} s	significant positions	value in (cm)
t_0	0.0	$x_0 = 0.00$	0.0
t_1	2.28	$x_1 = 0.001x_{max}$	3×10^{-3}
t_2	2.52	$x_2 = 0.004x_{max}$	1.2×10^{-2}
t_3	3.7	$x_3 = 0.019x_{max}$	5.7×10^{-2}
t_4	10	$x_4 = 0.033x_{max}$	0.1
		$x_5 = 0.60x_{max}$	1.797
		$x_6 = 0.80x_{max}$	2.39

Figure.4.2 presents calculated electron density as a function of distance from welded surface plate of times t_0, t_1, t_2, t_3, and t_4.

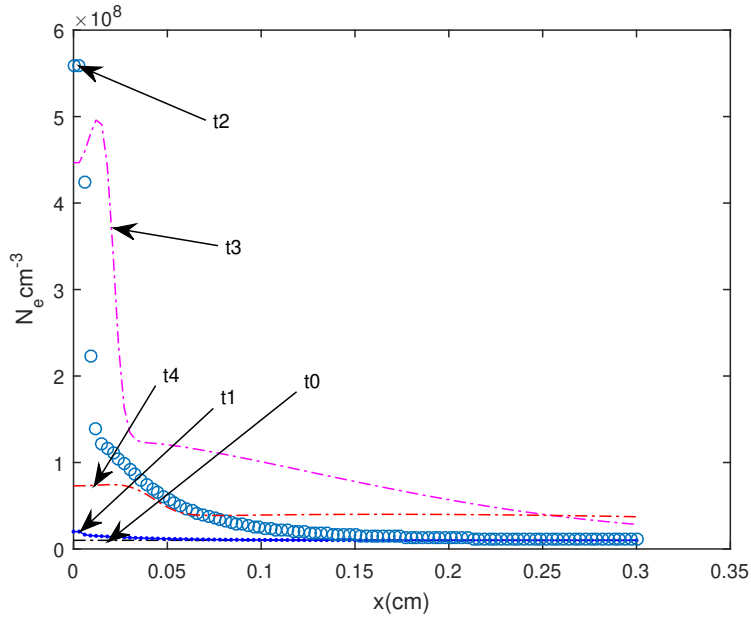

Figure 4.2 – *Electron density as a function of distance from the surface.*

Figure. 4.3 presents the calculated distributions of electron density as a function of times when the surface plate welded at five distances from the surface x_0, x_1, x_2, x_3, x_4.

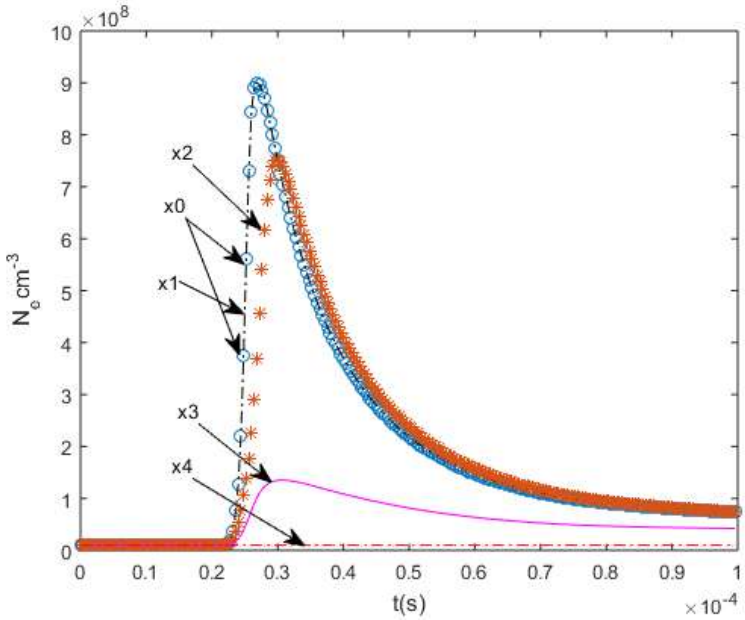

Figure 4.3 – *The electron density as a function of time for distances x_0, x_1, x_2, x_3, x_4.*

4.3 Temporal and spatial distribution of Temperatures and densities of species

Figures.4.4a, 4.4b, 4.5a and 4.5b show the profile of particle densities and temperatures as a function of time at the surface.

During the first phase corresponding to heating, the increase is very rapid. During the second cooling

phase (after the passage of the laser beam), the distributions are decreases; these variations are less rapid.

Also it can be seen that particle densities and temperatures has the same trend as surface temperature, when the surface temperature increase or decrease also the particle densities and temperatures increase or decrease at the same time approximately.

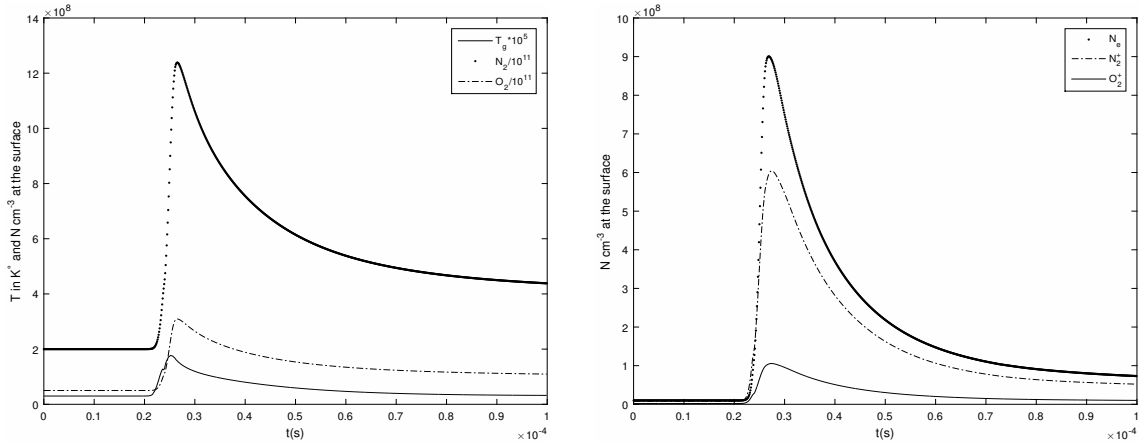

(a) *Gas temperature and neutral densities* (b) *Electron and ion densities*

Figure 4.4 – *Distributions of particle densities as a function of time at the surface.*

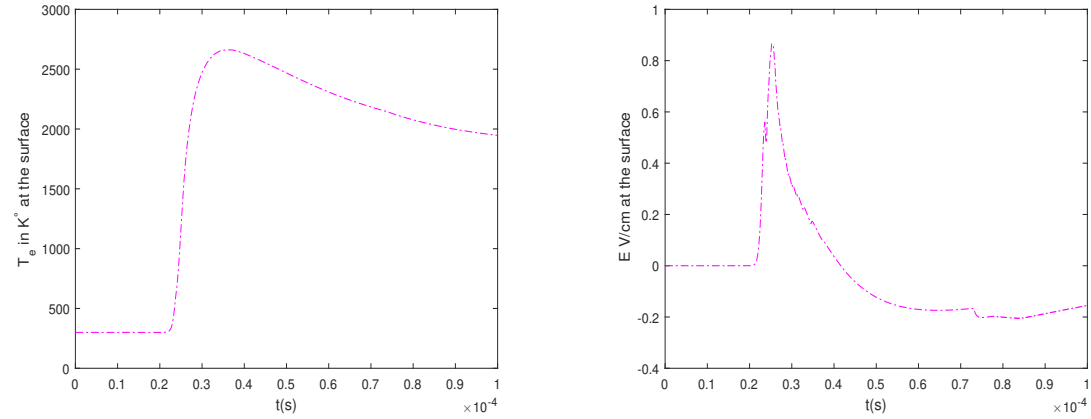

(a) *Electron temperature* (b) *Electric field*

Figure 4.5 – *Distributions as a function of time at the surface.*

Table. 4.2 presents the maximum values of species at specific points during laser welding. High population at near distances and low populations at points far from the surface for N_e, N_2^+, O_2^+, where for N_2 and O_2 has low population near the surface and high at long distances. We explain that by the ionization and electronic recombination.

Table 4.2 – *Maximum values of species in each specific positions during laser welding.*

x(cm)	T_g^{max} (K)	$N_{N_2}^{max}$ (10^{20}cm^{-3})	$N_{O_2}^{max}$ (10^{19}cm^{-3})	N_e^{max} (10^{8}cm^{-3})	$N_{N_2^+}^{max}$ (10^{8}cm^{-3})	$N_{O_2^+}^{max}$ (10^{8}cm^{-3})	T_e^{max} (K)
x_0	1772.2	1.2383	3.0913	9.004744	6.0432	1.0559	2661.1
x_1	1279.7	1.2383	3.0913	9.004811	6.0432	1.0559	2661.1
x_2	722.05	1.0417	2.6000	7.5184377	5.6534	0.98573	2663.2
x_3	334.00	2.2911	5.7258	1.3523757	1.2645	0.21801	2683.1
x_4	-	-	-	-	-	-	2726.6
x_5	-	-	-	-	-	-	787.8
x_6	-	-	-	-	-	-	370.6

Table. 4.3 shows that, at x_0 and x_1 the temperatures and particle densities reach the maximum value at the same time approximately.

Table 4.3 – *Time corresponding to maximum values of species in each specific distance during laser welding.*

x(cm)	t(10^{-5}s)						
	T_g^{max}	$N_{N_2}^{max}$	$N_{O_2}^{max}$	N_e^{max}	$N_{N_2^+}^{max}$	$N_{O_2^+}^{max}$(10^{-5}s)	T_e^{max}
x_0	2.5196	2.6531	2.6531	2.6856	2.7456	2.7411	3.6427
x_1	2.6261	2.6531	2.6531	2.6856	2.7456	2.7411	3.6427
x_2	3.5822	3.0917	3.0917	2.9911	2.7936	2.7916	3.6357
x_3	10.	10.	10.	3.0617	3.0077	3.0292	3.6402
x_4	-	-	-	-	-	-	3.6212
x_5	-	-	-	-	-	-	10.
x_6	-	-	-	-	-	-	10.

Figures. 4.6a, 4.6b, 4.7a and 4.7b show distributions of particle densities, temperatures and electric field as a function of space at the time when surface has a maximum temperature.

It can be seen that particle densities and temperatures has the same trend as surface temperature; when the surface temperature increase or decrease also the particle densities and temperatures increase or decrease at the same time approximately, it has the functional form of equation.4.1.

At t=0, the species has a sharp spike at the plate, but as time progresses, the distribution gets shorter and wider. In both coordinate systems, the energy spreads quickly at first when the species gradient is large and more slowly at later times when the gradients are smaller.

For the profiles of the density distributions of the various species, we were inspired by the shape of the concentrations due to the diffusion of matter on a surface. For ideal conditions these concentrations have the following form:

$$X(x,t) = \frac{1}{\sqrt{t}} \exp(-\frac{x^2}{4\alpha t}) \ . \tag{4.1}$$

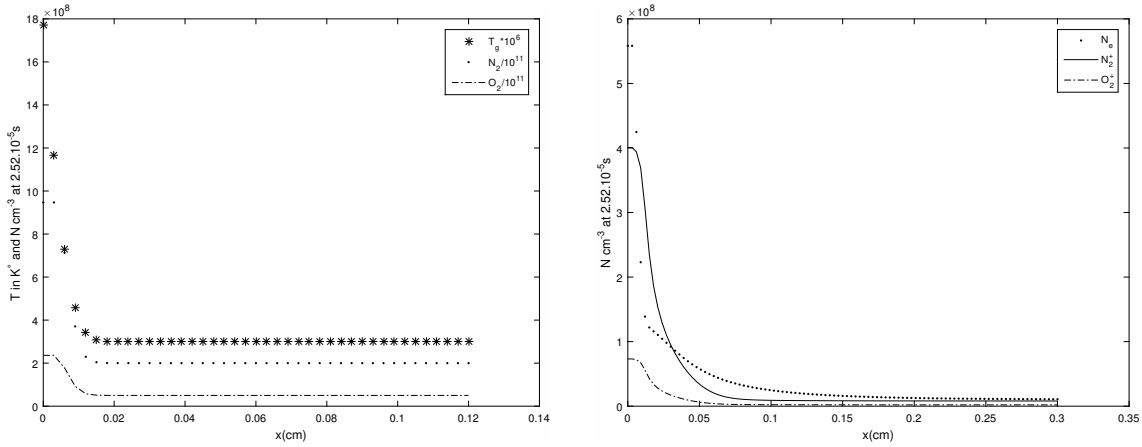

(a) *Gas temperature and neutral densities* (b) *Electron and ion densities*

Figure 4.6 – *Distributions of particle densities and temperatures as a function of space at the time when surface has a maximum temperature.*

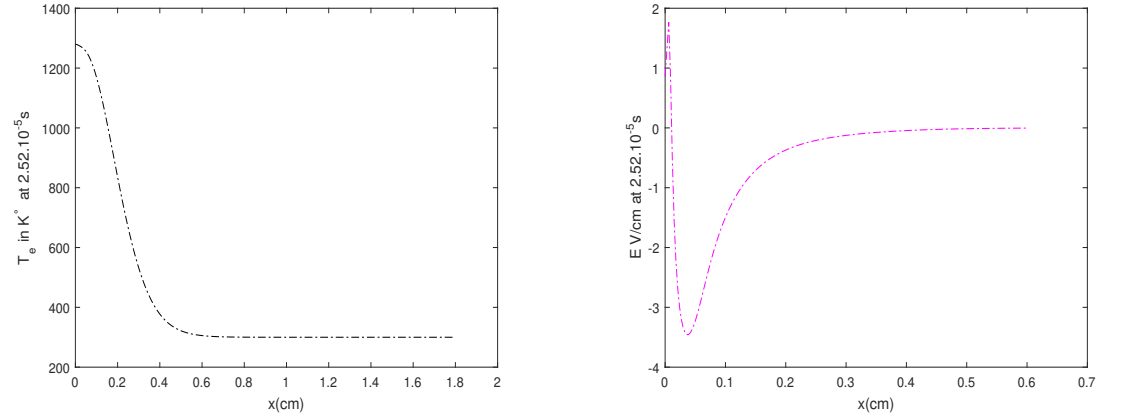

(a) *Electron temperature* (b) *Electric field*

Figure 4.7 – *Distributions of electron temperature and electric field as a function of space at the time when surface has a maximum temperature.*

From tables. 4.2 and 4.5 and from figures. 4.6a, 4.6b, 4.7a and 4.7b along the air at a point X_s, the species first increases, then slowly decays back to ambient state, when the surface temperature reach maximum value: $X_s \sim 0.02$ cm for (N_2, O_2, T_g), 0.06cm (N_2^+, O_2^+, N_e), 0.3 cm E and 0.5 cm T_e.

Table. 4.4 present the maximum values of species in each specific time during laser welding. The peak is directly proportional to the time until t_2 (the time when the surface reach the maximum temperature), after this point the peaks decreasing, except T_e which keep going up for longer period and than decreasing.

Table 4.4 – *Maximum values of densities and temperatures in each specific time t_1, t_2, t_3, t_4 during laser welding.*

t(s)	T_g^{max} (K)	$N_{N_2}^{max}$ (10^{20}cm^{-3})	$N_{O_2}^{max}$ (10^{19}cm^{-3})	N_e^{max} (10^{8}cm^{-3})	$N_{N_2^+}^{max}$ (10^{8}cm^{-3})	$N_{O_2^+}^{max}$ (10^{8}cm^{-3})	T_e^{max} (K)
t_1	900.6696	0.25604	0.63998	0.20102	0.3876476	0.8717958	357.35
t_2	17717	0.94677	2.3641	5.583	4.006584	7.3195016	1279.2
t_3	887.4417	0.89806	2.2419	4.9601	3.4549	0.61893	2972.
t_4	427.3018	0.44185	1.1035	0.74427	0.52242	0.10186	2431.3

Table 4.5 presents the position of x corresponding to the maximum values of densities and temperatures at four specific times during laser welding t_1, t_2, t_3, t_4. The value of x grows with the growth of time.

Table 4.5 – *Position of x corresponding to the maximum values of densities and temperatures in each specific time t_1, t_2, t_3, t_4 during laser welding.*

t(s)	x(cm)						
	T_g^{max}	$N_{N_2}^{max}$	$N_{O_2}^{max}$	N_e^{max}	$N_{N_2^+}^{max}$	$N_{O_2^+}^{max}$	T_e^{max}
t_1	0.00	0.00	0.00	0.003	0.00	0.00	0.00
t_2	0.00	0.00	0.00	0.003	0.00	0.00	0.003
t_3	0.00	0.012	0.012	0.012	0.012	0.012	0.3
t_4	0.024	0.018	0.018	0.021	0.015	0.012	0.74

Table 4.6 presents the points X_s at three specific times during laser welding t_1, t_2, t_3. X_s The value of X_s grows with the growth of time.

The values of X_s are different for the various parameters studied. The effect of the diffusion phenomenon plays a main role in the dynamics of these parameters: the mobility of electrons is faster and the diffusion of neutral molecules is the slowest.

Table 4.6 – *The point X_s at specific times during laser welding t_1, t_2, t_3.*

Species	X_s (cm)		
	at t=t_1	at t=t_2	at t=t_3
Ions and electrons	$0.795\lambda_D^1$	$1.65\lambda_D^2$	$8.639\ \lambda_D^3$
E	$5.30\lambda_D^1$	$8.26\lambda_D^2$	$15.118\lambda_D^3$
T_e	$10.61\lambda_D^1$	$13.77\lambda_D^2$	$28.07\lambda_D^3$

Where:

λ_D^1 :is Debye's length at t_1.

λ_D^2 :is Debye's length at t_2.

λ_D^3 :is Debye's length at t_3.

Table 4.7 presents plasma parameters at specific times t_1, t_2, t_3 during laser welding. Values of coupling parameter, $\Gamma_0 \ll 1$, show that the medium is a kinetic plasma. The average values of the periods of the electronic plasma oscillations ($T_{pl,osc} = \dfrac{2\pi}{\omega_p}$) are of the order of 10^{-8}s. These values are much lower than the characteristic times of the diffusion phenomena (10^{-5} and less than 10^{-4}s). The values of λ_D

are from 0.037 to 0.046 cm and R_s are of the order of 10^{-3}s, and Coulomb logarithm are from 9.9 to 11.24.

Table 4.7 – *Plasma parameters at the characteristic times of the diffusion phenomena of N_e, $T_e(s)$ during laser welding t_1, t_2, t_3.*

Plasma param.	Expression	Val.		
		at t=t_1 s	at t=t_2 s	at t=t_3 s
Debye's length λ_D [cm]	$6.9\sqrt{\frac{T_e[K]}{N_e[cm^{-3}]}}$	0.0377	0.0363	0.0463
Electronic plasma frequency $\omega_p\,[s^{-1}]$	$5.6.10^4\sqrt{N_e\,[cm^{-3}]}$	1.779×10^8	2.063×10^8	2.533×10^8
Coupling parameter Γ_0	$\frac{1}{12\pi N_e\lambda_D^3}$	4.90×10^{-5}	4.089×10^{-5}	1.307×10^{-5}
Particle distance R_S [cm]	$\sqrt[3]{\frac{3}{4\pi N_e}}$	0.0029	0.0026	0.0023
log. Coulomb $\ln\Lambda$	$\ln(12\pi N_e\lambda_D^3)$	9.9226	10.104	11.245
Period of electronic plasma oscillations $[s]$	$\frac{2\pi}{\omega_p}$	3.5318×10^{-8}	3.0456×10^{-8}	2.4805×10^{-8}

4.4 Analytical approach

The analytic solution of temperatures and particle densities equations takes the form [4]:

$$X_{e0}+\frac{(X_{eS}-X_{e0})}{\sqrt{4\pi D_X.(t-t_0)}}\exp(\frac{-(x_i+x_{eff})^2}{4\pi D_X.(t-t_0)}-10^4\mu_X E.(t-t_0))\ , \tag{4.2}$$

We used a Matlab program to determine the parameters of the functions to interpolate.
Using D_e, μ_e and E calculated in numerical solution and with $x_{eff}\sim0.0911$ cm, the electron density N_e at the surface $x_i=0$ takes the expression:

$$N_e=10^7+\frac{9.8\times10^7}{\sqrt{4\pi D_e.(t-t_0)}}\exp(\frac{-(0.0911)^2}{4\pi D_e.(t-t_0)}-2.3997.10^4(t-t_0))\ . \tag{4.3}$$

Qualitatively, the values of D_X, μ_X, E and x_{eff}, when used with Equation.4.2 for all temperatures and particle species, produce a graph very similar to numerical solution that is, the numerical and analytical values agree well up to the peak, but the analytic underestimates the heat loss and layer times and distance.

Typical results at the welded surface are shown in figure.4.8 together with the analytical formula. Note that the analytical solutions fit well at early times for each distance taken individually. They do not fit well when go back to ambient state.

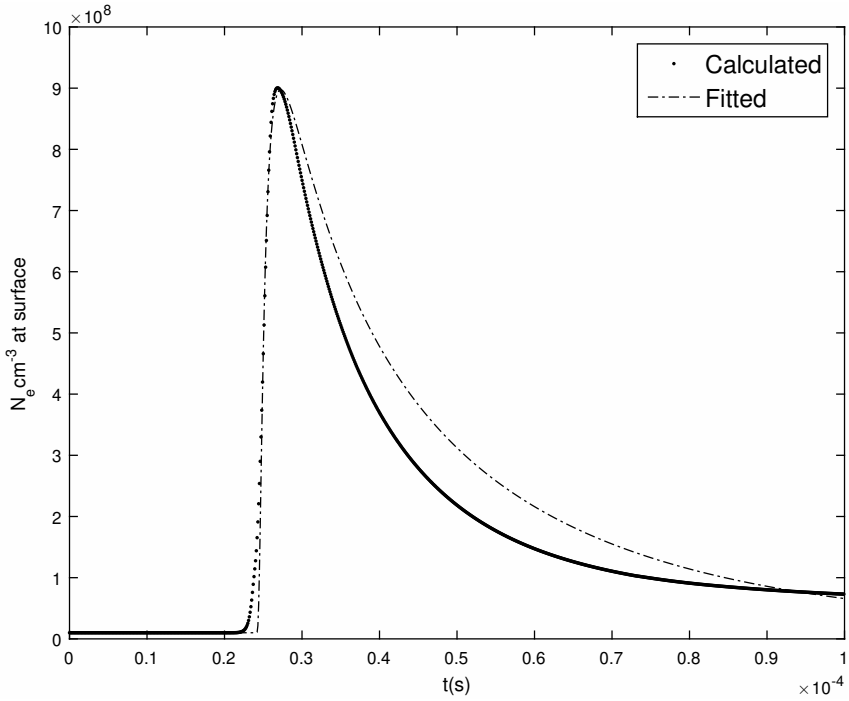

Figure 4.8 – *Calculated and fitted solution of electron density at the surface*

In order to obtain a very similar curve of electron density, we searched for more accurate expressions, we have divided the curve into two parts; heating and cooling part.
The analytic solution of electron density equation at the heating part is:

$$N_e^{Heating} = 10^7 + \frac{9.8 \times 10^7}{\sqrt{4\pi D_e.(t-t_0)}} \exp\left(\frac{-(0.0911)^2}{4\pi D_e.(t-t_0)} - 2.3997.10^4(t-t_0)\right) , \tag{4.4}$$

where: D_e is the mean value of electron diffusion at the surface $D_e = 350cm^2/s$, $t_0 = 2.35 \times 10^{-5}s$.
The analytic solution of electron density equation at the cooling part is:

$$N_e^{Cooling} = 10^7 + \frac{4.5 \times 10^7}{\sqrt{4\pi D_e.(t-t_0)}} \exp\left(\frac{-(0.044)^2}{4\pi D_e.(t-t_0)} - 10^4(t-t_0)\right) . \tag{4.5}$$

where: $D_e = 350cm^2/s$, $t_0 = 2.5 \times 10^{-5}s$.
Figure 4.9 shows The analytic solution of electron density equation at the heating and cooling part approximated to numerical calculation of electron density at the surface.

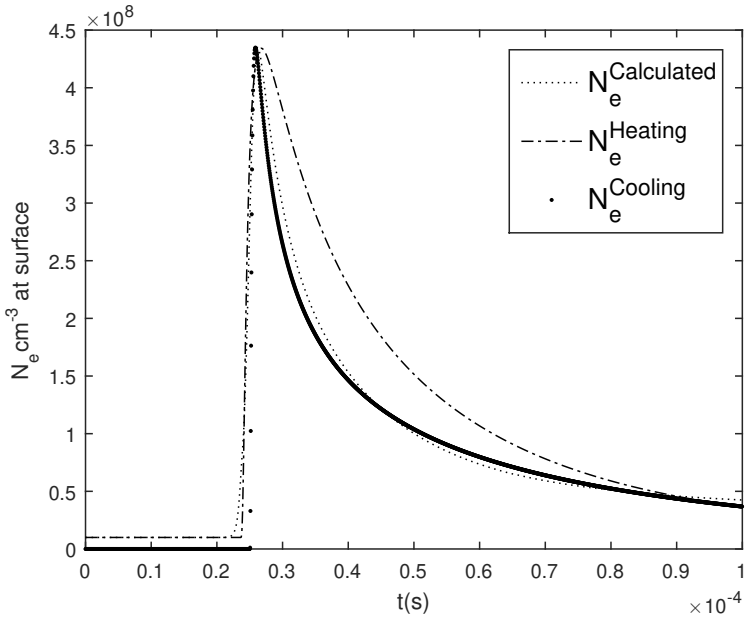

Figure 4.9 – *Heating and cooling approximated to numerical calculation of electron density at the surface*

4.5 Conclusion

The presented results for a numerical model adopted to simulate the heat transfer at the time when a surface plate welded. Through analyzing the result, it is found that, the induced air plasma can provide high energy electrons and it is favorable to ionize the gas. It also can provide internal electric field at the order of 1 V/cm and electron density at the order 9×10^8 cm^{-3} and electron temperature at the order 3000 K. A spatial and temporal distribution of thermal and particular density are presented and discussed; we found that the profile is a Gaussian in the distance x and decreases in amplitude and increases in width with increasing time. Along the air at a specific point X_s the species first increases, then slowly decays back to ambient state. Also it can be seen that particle densities and temperatures has the same trend as surface temperature, when the surface temperature increase or decrease also the particle densities and temperatures increase or decrease at the same time approximately. In both coordinate systems, the energy spreads quickly at first when the species gradient is large and more slowly at later times when the gradients are smaller. We also suggests an analytic approach to our numerical solution for electron density by the help of analytic formulas of [4], typical results at the welded surface are shown in figure.4.8 together with the analytic formula. Note that the analytic solutions fit well at early times for each distance taken individually. They do not fit well when go back to ambient state.

The numerical model shows varies results for the temporal and spatial distributions of electron densities close to the surface during the welding process.

Chapter 5

Stark broadening of isolated lines

5.1 Introduction

In this chapter we calculate Stark widths for isolated lines of the non hydrogenic heavy element Mg I. We calculate the contributions of weak collisions and strong collisions using two limiting cases for impact parameter. In order to study the validation of this new estimated formula for other spectral lines in other atoms, we calculate electronic Stark widths for the two atoms in the same column in periodic table Be I and Ca I, using the same plasma conditions. We analyse the electron density dependence for Be I, Mg I and Ca I spectral lines one time at v_c constant and other time at T_e constant. Finaly, we presented and discussed a comparison between our result with the theoretical and the experimental results of Griem (1974) [14] , STARK-B web site [13] and Dimitrijević and Sahal-Bréchot (1994) results [9].

5.2 Electron Broadening for Mg I

Table 5.1 presents the critical velocity V_c for some upper levels of Mg I transitions.

Table 5.1 – *Critical velocity V_c for some upper levels Mg I transitions.*

Wavelengths	Transitions	V_c(cm/s)
2025.824 Å	4p ^{1}P - 3s ^{1}S	8.90×10^7
4702.990 Å	5d ^{1}D - 3p ^{1}P	7.11×10^7
5167.732 Å	4s ^{3}S - 3p ^{3}P	9.97×10^7
5528.404 Å	4d ^{1}D - 3p ^{1}P	7.64×10^7
2852.127 Å	3p ^{1}P - 3s ^{1}S	9.14×10^7

Table 5.2 presents the electrons impact half-widths (HWHM: Half Width at Half Maximum) for Mg

I lines for a temperature $T_e = 20000K$ and the electron density $N_e = 10^{16}\ cm^{-3}$: for our calculation (ϕ^{Our}) and those of Griem(1974) (ϕ^{G74}) and STARK-B web site values (ϕ^{SB}) [13, 14].

Table 5.2 – *Electron impact half-widths ϕ, for Mg I lines, for our calculation and those of Griem (1974) and STARK-B web site.*

Wavelengths	Transitions	ϕ^{Our}(Å)	ϕ^{G74} (Å)	ϕ^{SB}(Å)	ϕ^{G74}/ϕ^{Our}	ϕ^{SB}/ϕ^{Our}
2025.824 Å	4p ^{1}P - 3s ^{1}S	0.0247	0.0158	0.0245	63.96%	99.19%
4702.990 Å	5d ^{1}D - 3p ^{1}P	1.036	0.612	0.885	59.07%	85.42%
5167.732 Å	4s ^{3}S - 3p ^{3}P	0.0474	0.0383	0.0582	80.80%	122.7%
5528.404 Å	4d ^{1}D - 3p ^{1}P	0.431	0.282	0.424	65.42%	98.37%

In table 5.2, the ratio of our calculation and those of Griem (1974) [14] is about (59.07-80.80%) and (85.42-122.7%) with STARK-B website [13] at $20000K$ and the electron density $N_e = 10^{16}\ cm^{-3}$; generally, our calculated values are greater. We must notice here, that our result is based on the broadening of the upper level of the transition, whereas those of Griem (1974) [14] and STARK-B web site [13] on the broadening of the upper and lower levels. We have contented ourselves with considering only the broadening of the upper level. We have verified, for these transitions, that the broadening of the lower levels is negligible. The table 5.3 shows the ratio between the electronic broadening of lower to upper levels. Because of the large energy gap between the upper and lower levels, we can consider that each group of levels (upper or lower) is broadened separately.

Table 5.3 – *Ratio of the electron broadening of lower level and upper level.*

Wavelengths	Transitions	ϕ^{Upper}	ϕ^{Lower}	$\phi^{Lower}/\phi^{Upper}$
2025.824 Å	4p ^{1}P - 3s ^{1}S	0.247×10^{-1}	4.234×10^{-5}	0.17%
4702.990 Å	5d ^{1}D - 3p ^{1}P	1.036	9.06×10^{-3}	0.87%
5167.732 Å	4s ^{3}S - 3p ^{3}P	0.0474	—	—
5528.404 Å	4d ^{1}D - 3p ^{1}P	0.431	1.25×10^{-2}	2.9%

The calculations show that the upper levels are more broadened than the lower levels. In table 5.3 the ratio between the electronic broadening of lower to upper levels is less than 3%, So it is sufficient to keep a few neighbor states for upper level; we neglected contribution of lower level and the term of interference.

Table 5.4 presents a comparison between experimental $\Delta\lambda_{mes}$ Stark full widths (FWHM: Full Width at Half Maximum) of Dimitrijević & Sahal-Bréchot (1994) [9] and our theoretical full widths $\Delta\lambda_{cal}$ in Angstrom units for some Mg I lines. The comparison shows an acceptable agreement between the results.

Table 5.4 – *Comparison between experimental $\Delta\lambda_{mes}$ Stark full widths (FWHM) of Dimitrijević and Sahal-Bréchot (1994) and our theoretical full widths $\Delta\lambda_{cal}$ in Angstrom units for some Mg I lines.*

Wavelengths	Transitions	T(K)	$N_e(10^{17}cm^{-3})$	$\Delta\lambda_{mes}$(Å)	$\Delta\lambda_{cal}$(Å)	$\Delta\lambda_{mes}/\Delta\lambda_{cal}$
4702.990 Å	5d ^{1}D - 3p ^{1}P	10000	1	8.33	11.44	72.81%
5528.404 Å	4d ^{1}D - 3p ^{1}P	10000	1	3.87	4.60	84.13%
2852.127 Å	3p ^{1}P - 3s ^{1}S	12970	1.1	0.0409	0.0579	70.63%

Table 5.5 presents the ratio of weak to the strong contribution on electronic width for some transitions at electronic density $N_e = 10^{16}\ cm^{-3}$ and various values of temperature.

Table 5.5 – *The ratio of weak collisions to the strong collisions as a function of temperature.*

T(K)	$\phi_{Weak}/\phi_{Strong}$			
	4p ^{1}P - 3s ^{1}S	5d ^{1}D - 3p ^{1}P	4s ^{3}S - 3p ^{3}P	4d ^{1}D - 3p ^{1}P
5000	12.93	5.42	8.86	8.18
10000	5.77	3.49	4.72	4.04
20000	4.39	3.16	3.51	3.27
30000	4.19	3.14	3.39	3.16
40000	4.14	3.12	3.41	3.14

Table 5.6 presents the ratio of electronic width of our results and those of Griem (1974) and STARK-B website as a function of temperature for some transitions at electronic density $N_e = 10^{16}\ cm^{-3}$ and various values of temperature.

Table 5.6 – *The ratio of electronic width of our results and those of Griem (1974) and STARK-B website as a function of temperature.*

T(K)	4p ^{1}P - 3s ^{1}S		5d ^{1}D - 3p ^{1}P		4s ^{3}S - 3p ^{3}P		4d ^{1}D - 3p ^{1}P	
	$\frac{\phi_{G74}}{\phi_{Our}}$	$\frac{\phi_{SB}}{\phi_{Our}}$	$\frac{\phi_{G74}}{\phi_{Our}}$	$\frac{\phi_{SB}}{\phi_{Our}}$	$\frac{\phi_{G74}}{\phi_{Our}}$	$\frac{\phi_{SB}}{\phi_{Our}}$	$\frac{\phi_{G74}}{\phi_{Our}}$	$\frac{\phi_{SB}}{\phi_{Our}}$
5000	4.23	7.87	2.41	4.04	13.04	21.19	2.91	4.99
10000	1.21	2.05	0.94	1.44	2.23	1.62	1.10	1.74
20000	0.64	0.99	0.59	0.85	0.69	1.51	0.65	1.50
30000	-	0.79	-	0.74	-	0.83	-	0.82
40000	0.47	-	0.46	-	0.48	-	0.49	-

In figure. 5.1, we present the variation of the ratio of the weak to strong contribution for some transitions at electron density $N_e = 10^{16}\ cm^{-3}$ and as a function of temperature.

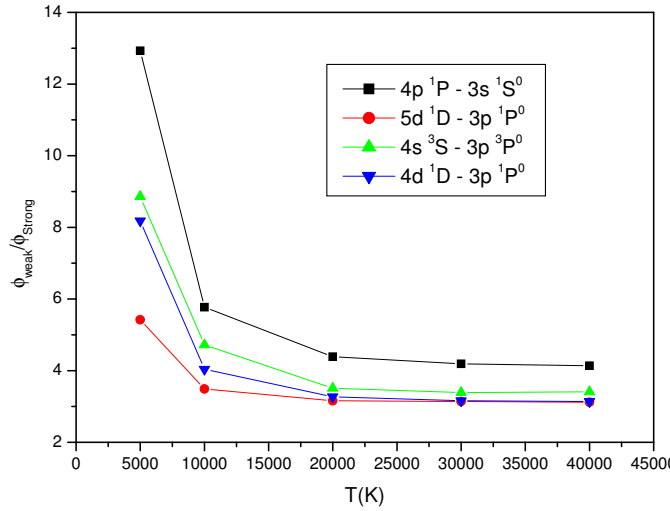

Figure 5.1 – *Variation of the ratio of weak collisions to the strong collisions as a function of temperature for some transitions.*

We see in figure. 5.1 and table 5.5 that there are two regions; for temperatures of the order of 5000K this ratio is very high and for temperatures from 10000K to 40000K this ratio varies from 3 to 6 for $\phi^{Weak}/\phi^{Strong}$, it confirm the importance of contribution of weak term and the use of strong term as correction.

In figures. 5.2a and 5.2b, we present the ratio of electronic width as a function of temperature for some transitions of our results and those of a) Griem (1974) [14], b) STARK-B web site [13].

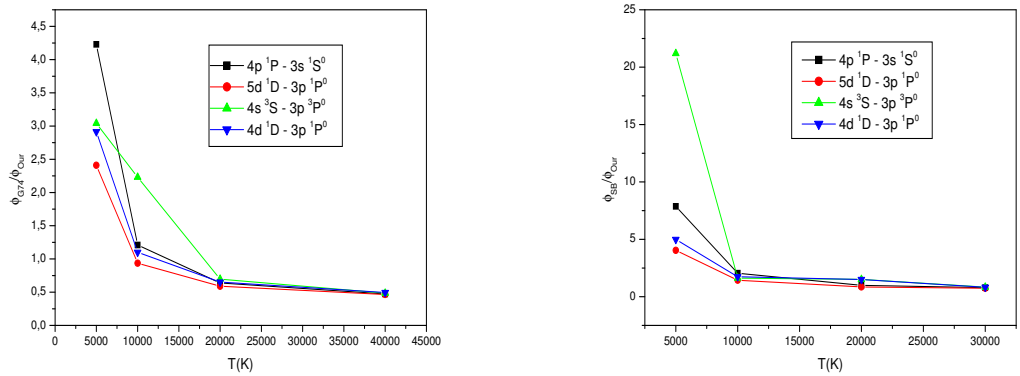

(a) *our results and those of STARK-B web site* (b) *our results and those of Griem (1974)*

Figure 5.2 – *Variation of the ratio of electronic width as a function of temperature for some transitions.*

We see in table 5.6 and figures. 5.2a and 5.2b that for temperatures of the order of 5000K the calculated width is smaller than those of Griem (1974) [14] and Stak-B [13]. For temperatures from $10000K$ to $40000K$, the calculated width is generally in the same order of values of Griem (1974) [14] and Stark-B [13]. For $T_e = 20000K$, we have nearest values between the three models.

5.3 Electron Broadening for other neutral atoms Be I and Ca I

In order to study of validation of the new estimated formula in [7] for other spectral lines in other atoms, we chose the two atoms in the same column in periodic table Be I and Ca I.

In figures. 5.3, 5.4 and 5.5, we present a comparison between Be I, Mg I, Ca I with Griem 1974 (G74) [14] and Stark-B web site (SB) [13] at $N_e = 10^{16} cm^{-3}$ for transitions Be I ($\lambda = 4573$Å 2p-3d $^1P - ^1D$) and Mg I ($\lambda = 4703$Å 3p-5d $^1P - ^1D$) and Ca I ($\lambda = 4427$Å 4s-4p $^1S - ^1P$).

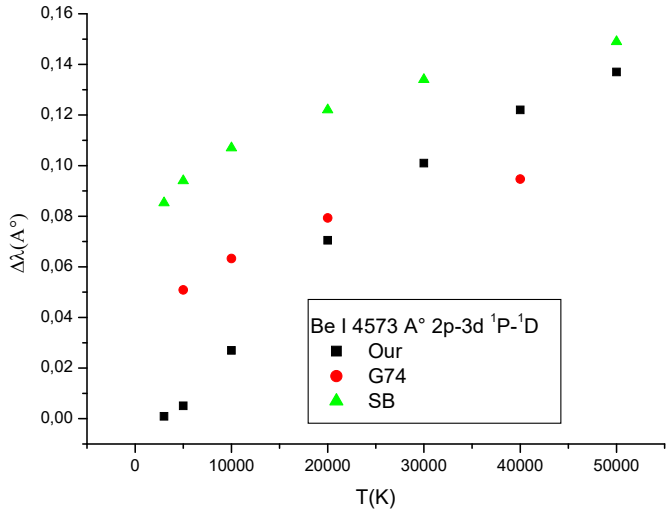

Figure 5.3 – *Comparison of Stark broadening at* $N_e = 10^{16} cm^{-3}$ *with (G74) and SB for Be I.*

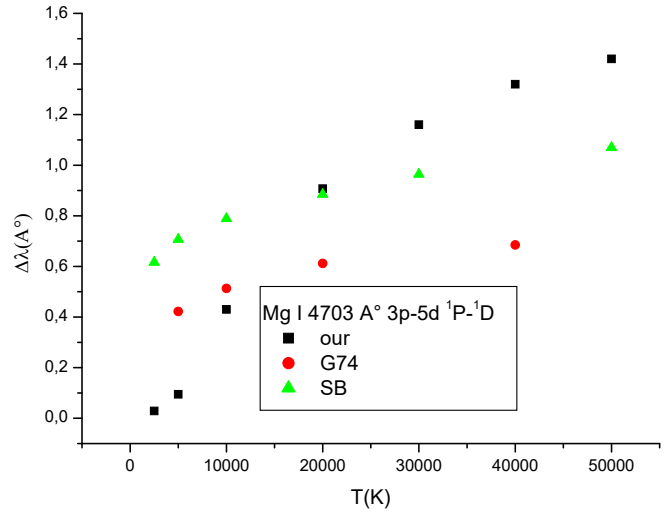

Figure 5.4 – *Comparison of Stark broadening at* $N_e = 10^{16} cm^3$ *with (G74) and SB for Mg I.*

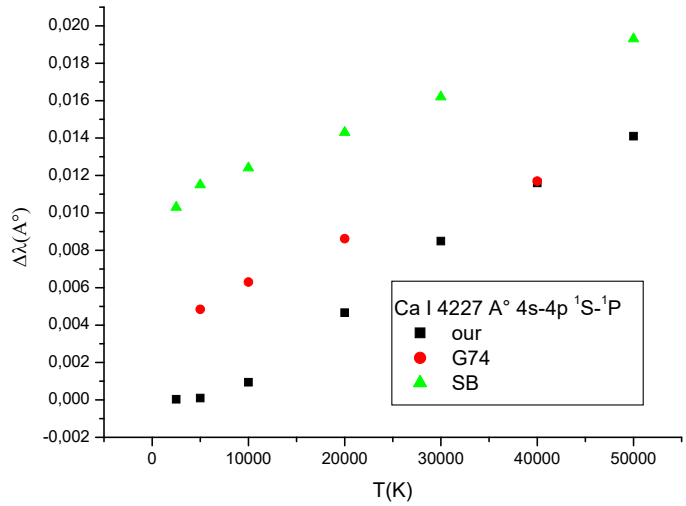

Figure 5.5 – *Comparison of Stark broadening at* $N_e = 10^{16} cm^3$ *with (G74) and SB for Ca I.*

We see in figures. 5.3,5.4 and 5.5 that our results for beryllium and calcium are also agree nearly with those of Griem (1974) [14] and those of STARK-B web site [13]. For Be I, Mg I and Ca I spectral lines, we have found that the three lines have the same temperature dependence in the same plasma conditions.

In figure. 5.6, we present the variation of Stark broadening with electron density for Be I, Mg I, Ca I at $v_c = 1$.

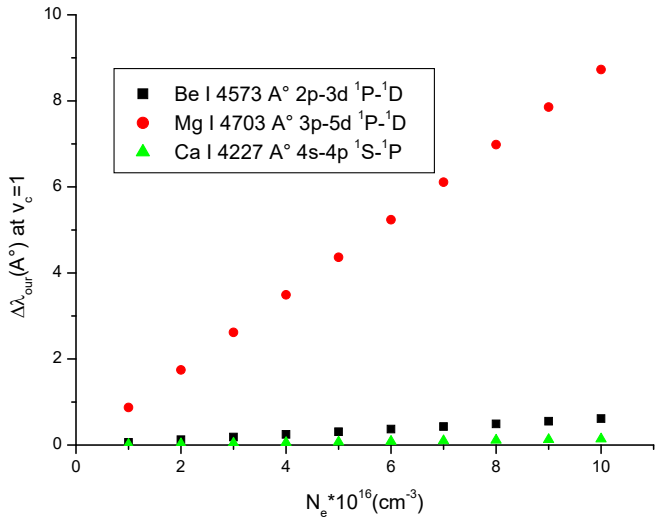

Figure 5.6 – *Variation of Stark broadening with electron density at $v_c = 1$ for Be I, Mg I and Ca I.*

In figure. 5.7, we present the variation of Stark broadening with electron density for Be I, Mg I, Ca I at $T_e = 20000$ K.

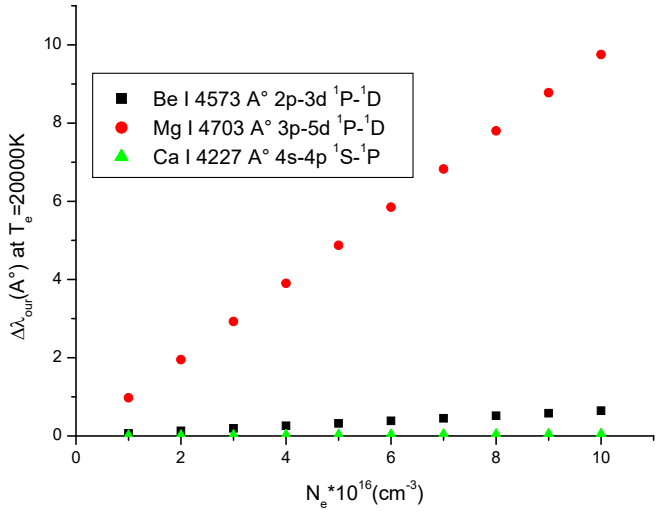

Figure 5.7 – *Variation of Stark broadening for Be I, Mg I and Ca I at $T_e = 20000K$.*

In figures. 5.6 and 5.7 we analyse the electron density dependence for Be I, Mg I and Ca I spectral lines one time at v_c constant and other time at T_e constant, we have found that the electronic broadening

Be I, Mg I and Ca I spectral lines has a linear variation with electron density. Our formula is very useful for isolated lines of Be I and Ca I in temperature range 10000 K to 50000 K.

5.4 Stark broadening of Mg I in welding conditions

In our welding conditions, Stark broadening calculations have been carried out on low electron density ($N_e \leq 10^9 cm^{-3}$) and low electron temperature ($T_e \leq 3000K$) and relatively low gas temperature ($T_g \leq 1800K$), under atmospheric pressure. A Stark broadening at T_e= 2500 K of STARK-B web site [13] is extrapolated from $N_e = 10^{11} cm^{-3}$ to $N_e = 10^9 cm^{-3}$; electron impact widths and shifts are linear in N_e [14].

Table 5.7 – *Electron impact half-widths ϕ, for Mg I lines under welding conditions at maximum electron density $N_e = 10^9 cm^{-3}$, for our calculation and those of STARK-B web site.*

Wavelengths	Transitions	T(K)	ϕ^{Our}(Å)	ϕ^{SB} (Å)	ϕ^{Our}/ϕ^{SB}
2025.824 Å	4p ^{1}P - 3s ^{1}S	2500	3.0×10^{-11}	1.63×10^{-10}	18.40%
		3000	5.3×10^{-11}	_	_
4702.990 Å	5d ^{1}D - 3p ^{1}P	2500	3.0×10^{-9}	6.17×10^{-9}	48.62%
		3000	4.9×10^{-9}	_	_
5167.732 Å	4s ^{3}S - 3p ^{3}P	2500	2.7×10^{-11}	3.88×10^{-10}	6.95%
		3000	4.2×10^{-11}	_	_
5528.404 Å	4d ^{1}D - 3p ^{1}P	2500	1.2×10^{-9}	3.00×10^{-9}	40.%
		3000	2.0×10^{-9}	_	_

The results in Table 5.7 show a difference within (6.95%-48.62%) with STARK-B web site [13].

Table 5.8 – *A comparison between Stark broadening $\Delta\lambda_S$ and Doppler broadening $\Delta\lambda_D$, for Mg I lines under welding conditions.*

Wavelengths	Transitions	T(K)	$\Delta\lambda_S$ (Å)	$\Delta\lambda_D$(Å)	$\Delta\lambda_S/\Delta\lambda_D$
2025.824 Å	4p ^{1}P - 3s ^{1}S	2500	3.0×10^{-11}	1.48×10^{-2}	$\sim 10^{-9}$
		3000	5.3×10^{-11}	1.62×10^{-2}	$\sim 10^{-9}$
4702.990 Å	5d ^{1}D - 3p ^{1}P	2500	3.0×10^{-9}	3.44×10^{-2}	$\sim 10^{-7}$
		3000	4.9×10^{-9}	3.77×10^{-2}	$\sim 10^{-7}$
5167.732 Å	4s ^{3}S - 3p ^{3}P	2500	2.7×10^{-11}	3.78×10^{-2}	$\sim 10^{-9}$
		3000	4.2×10^{-11}	4.14×10^{-2}	$\sim 10^{-9}$
5528.404 Å	4d ^{1}D - 3p ^{1}P	2500	1.2×10^{-9}	4.04×10^{-2}	$\sim 10^{-7}$
		3000	2.0×10^{-9}	4.43×10^{-2}	$\sim 10^{-7}$

In Table 5.8 the result show that, in these conditions, the Stark broadening is negligible comparing with Doppler broadening, so the profiles can be assumed to be purely Gaussian.

So, we can conclude that the profiles of isolated lines of Mg I will be a good tool to evaluate gas temperature. A more exact calculation of the profile required an integrated calculation over space and time according to the gas dynamics near the welding surfaces. Indeed, the measurements require the integration on the lines of sight of the spectrometers (rapid variation along x) and require the integration over time if the time taken for images by the spectrometers are long. The atoms and the ions of magnesium are present in the form of traces and must not affect too much the dynamics of the gas mixture O_2/N_2 (subject of chapter 4).

5.5 Conclusion

We calculate Stark widths for isolated lines of the non hydrogenic heavy element Mg I. We have used a simple formula that we have developed from a formula of electronic broadening in [71]. We calculate the contributions of weak collisions and strong collisions using two limit case for impact parameter. Our formula agrees within (59.07-80.80%) with Griem's results [14] and agrees with (85.42-122.7%) with STARK-B website [13] at 20000 K. For the temperature range 10000-50000 K, our results are also agree nearly with those of Griem (1974) [14] and those of STARK-B website [13]. The comparison between our result and experimental measurements of Dimitrijević and Sahal-Bréchot (1994) [9] shows that it agrees within (70.63-84.13%). In this method, it is sufficient to keep a few neighbor states for upper level; we neglected contribution of lower level and the term of interference. Note that the proposed model can be used, without limitation, to express separately the electronic broadening of the top and bottom levels by neglecting the terms of interference between the two subsystems. In order to study the validation of this new estimated formula for other spectral lines in other atoms, we calculate electronic Stark widths for the two atoms in the same column in periodic table Be I and Ca I, using the same plasma conditions. Our results for beryllium and calcium are also agree nearly with those of Griem (1974) [14] and those of STARK-B web site [13]. We analyse the electron temperature dependence for Be I, Mg I and Ca I spectral lines, we have found that the three lines have the same temperature dependence in the same plasma conditions. We analyses the electron density dependence for Be I, Mg I and Ca I spectral lines one time at v_c constant and other time at T_e constant, we have found that the electronic broadening has a linear variation with electron density. Our formula is very useful for isolated lines of Be I and Ca I in temperature range 10000 K to 50000 K.

In order to calculate Stark broadening under welding conditions, we use our formula and STARK-B web site [13] result. The results show a difference within (6.95%-48.62%) with STARK-B web site [13]. These conditions, the Stark broadening is negligible comparing with Doppler broadening; and the profiles of isolated lines of Mg I will be a good tool to evaluate gas temperature.

Calculation of Stark Broadening line due to non hydrogenic electrons for several plasma media.

General conclusion and perspectives

Physical systems naturally evolve toward higher entropy states. Hence, thermal diffusion is a direct result of the logical operation of the universe [3].

In this thesis, we are interested in the study of a gas mixture (O_2 / N_2) near a metal surface during laser welding. The surface of the metal is brought to a temperature varying with time, we calculated the spatial and temporal distributions of temperatures and densities of molecules (O_2 and N_2), ions (O_2^+ and N_2^+) and electrons.

We used the fluid model coupled to the Poisson's equation for electric charges. We use the Exponential Scheme (SG Scheme) to resolve the densities of electrons and ions and the electron energy (electron temperature). For numerical resolution of the gas temperature and neutral density equations, we use the Finite Difference Method (FDM), the nonlinear coupled equations have matrix forms and iterative technique is used to find solutions.

In many processes, such as the arc welding and laser welding, a luminous gas plasma forms near the weld pool. In welding process, the luminosity of the plasmas is a very important property.

The spectroscopic diagnosis by spectral lines can be very useful tools for understanding phenomena. These spectral lines can be broadened by Stark broadening (electronic and ionic) or by other causes. We describe simple method for calculation the contribution of electrons to the broadening using impact theory with a model based on two limits case for reduced velocity for ($v_c < 1$) and for ($v_c > 1$).

In chapter 1, we have presented the main elements relating to the main themes addressed.

In chapter 2, we have established (1D) fluid model contains a set of gas dynamics equations, at atmospheric pressure in the presence of air during laser welding, for plasma gas temperature, electron energy (electron temperature), charged and neutral species densities. We have described the basic mathematical equations of our model.

In chapter 3, we presented a theoretical implementation to obtain the minimum of the impact parameter for strong and weak contribution in collision operator. We also presented the contribution of strong collision and weak collision respectively for magnesium neutral emitters. We neglect the contribution of ion to the broadening to the widths of isolated lines; ion contribution is usually less than 20% for many spectral lines. Practically all the broadening is caused by interactions between the upper state of the line in question and its neighbors, and lower state interactions can be neglected [72].

In chapter 4, we presented and discussed the calculated spatial and temporal distributions of species near the surface (N_2, O_2, N_2^+, O_2^+ and electrons and temperatures), during laser welding of magnesium alloy.

We calculate the temporal and spatial distributions of densities and temperatures near the surface during laser welding of magnesium alloy. The induced air plasma can provide high energy electrons

and it is favorable to ionize the gas. It can provide internal electric field at the order of 1 V/cm and electron density at the order 9×10^8 cm^{-3}, and electron temperature at the order 3000 K. Also it can be seen that particle densities and temperatures has the same trend as surface temperature; when the surface temperature increase or decrease also the particle densities and temperatures increase or decrease at the same time approximately.

In chapter 5, we presented the calculated full Stark width (ionic and electronic) of isolated lines Mg I, Be I and Ca I. A comparison between our result with the theoretical and the experimental results of Griem (1974) [14], STARK-B web site [13], Dimitrijević and Sahal-Bréchot (1994) results [9], we presented Stark broadening of Mg I under welding conditions. We calculate the contributions of weak collisions and strong collisions using two limiting cases for impact parameter. Our formula is in good agreement with Griem's results [14] and STARK-B website results [13] at 20000 K. For the temperature range (10000-50000 K), our results are also agree nearly with those of Griem (1974) [14] and those of STARK-B web site [13], the comparison between our result and experimental measurements of Dimitrijević and Sahal-Bréchot (1994) [9] also shows a good agreement. In this method, it is sufficient to keep a few neighbor states for upper level; we neglected the contribution of lower level and the term of interference. Note that the proposed model can be used, without limitation, to express separately the electronic broadening of the top and bottom levels by neglecting the terms of interference between the two subsystems.

In order to study of validation of the new estimated formula for other spectral lines in other atoms, We calculate Stark broadening for the two atoms in the same column in periodic table Be I and Ca I,using the same plasma conditions. Our results for beryllium and calcium are also agree nearly with those of Griem (1974) [14] and those of STARK-B web site [13].

For Be I, Mg I and Ca I spectral lines, we have found that the three lines have the same temperature dependence in the same plasma conditions. We analyse the electron density dependence for Be I, Mg I and Ca I spectral lines one time at v_c constant and other time at T_e constant, we have found that the electronic broadening Be I, Mg I and Ca I spectral lines has a linear variation with electron density. Our formula is very useful for isolated lines of Be I and Ca I in temperature range 10000 K to 50000 K. In order to calculate Stark broadening under welding conditions, we used our formula and STARK-B web site result [13]. The results show a defference within (6.95%-48.62%) with STARK-B web site [13]. Under these conditions Stark broadening is negligible comparing with Doppler broadening; and the profiles of isolated lines of Mg I will be a good tool to evaluate gas temperature.

Perspectives

The perspectives for this work include the following points:

1. Using temperatures near the surface metal higher than those studied in this thesis.
2. Studying fluid model for 2 or 3 dimensions.
3. More detailed integrated calculation over time and space of spectral line profiles.

4. Studying fluid model in the presence of shielding gas.

5. Calculating or investigating Stark broadening for ions and other heavy species.

6. Microscopic study of limit conditions relating to inelastic electronic collision at surfaces.

Bibliography

[1] W. Yi-Nan, L. Yue, and L. Guo-Qiang. A computational study of radio frequency atmospheric pressure discharge in nitrogen and oxygen mixture gases. *Chinese Physics Letters*, 30(3):035201, 2013. (Cited page 1.)

[2] W. Yi-Nan and L. Yue. Numerical study on characteristics of radio-frequency discharge at atmospheric pressure in argon with small admixtures of oxygen. *Plasma Science and Technology*, 19(7):075402, 2017. (Cited page 1.)

[3] T. Gfroerer, R. Phillips, and P. Rossi. Thermal diffusivity imaging. *American Journal of Physics*, 83(11):923–927, 2015. (Cited pages 1, 26, and 58.)

[4] M. C. Sullivan, B. G. Thompson, and A. P. Williamson. An experiment on the dynamics of thermal diffusion. *American Journal of Physics*, 76(7):637–642, 2008. (Cited pages 1, 8, 46, and 48.)

[5] J. Hoffman, Z. Szymański, and V. Azharonok. Plasma plume induced during laser welding of magnesium alloys. In *AIP Conference Proceedings*, volume 812, pages 469–472. American Institute of Physics, 2006. (Cited pages 1 and 4.)

[6] L. Liu and X. Hao. Study of the effect of low-power pulse laser on arc plasma and magnesium alloy target in hybrid welding by spectral diagnosis technique. *Journal of Physics D: Applied Physics*, 41(20):205202, 2008. (Cited pages 1, 3, and 21.)

[7] Y. Ben Nana, F. Khelfaoui, M. T. Meftah, and E. S. Lari. A novel investigation in the electronic broadening of spectral line profiles: Application to neutral magnesium in plasmas. *Optik*, 202:163485, 2020. (Cited pages 1, 2, 14, 16, 21, and 53.)

[8] S. A. Freudenstein and J. Cooper. A simple formula for estimating stark widths of neutral lines. *The Astrophysical Journal*, 224:1079–1084, 1978. (Cited page 2.)

[9] M. S. Dimitrijevic and S. Sahal-Bréchot. Stark broadening parameter tables for mg i lines of interest for solar and stellar spectra research. i. *Bulletin Astronomique de Belgrade*, 149:31–84, 1994. (Cited pages 2, 49, 50, 57, and 59.)

[10] M. S. Dimitrijevic and N. Konjevic. Simple formulae for estimating stark widths and shifts of neutral atom lines. *Astronomy and Astrophysics*, 163:297–300, 1986. (Cited page 2.)

[11] B. Zmerli, N. Ben Nessib, and M. S. Dimitrijević. Temperature dependence of atomic spectral line widths in a plasma. *The European Physical Journal D*, 48(3):389–395, 2008. (Cited pages 2 and 16.)

[12] S. Sahal-Bréchot, M. S. Dimitrijević, and N. Ben Nessib. Comparisons and comments on electron and ion impact profiles of spectral lines. *Open Astronomy*, 20(4):523–530, 2011. (Cited page 2.)

[13] S. Sahal-Bréchot, M. S. Dimitrijević, and N. Moreau. Stark-b database. *Observatory of Paris, LERMA and Astronomical Observatory of Belgrade. URL:* `http://stark-b.obspm.fr[March, 2019]` , 2019. (Cited pages 2, 18, 49, 50, 52, 53, 55, 56, 57, and 59.)

[14] H. R. Griem. *Spectral Line Broadening by Plasmas Academic Press*. 1974. (Cited pages 2, 18, 30, 31, 32, 37, 49, 50, 52, 53, 55, 56, 57, and 59.)

[15] L. Liu and X. Hao. Improvement of laser keyhole formation with the assistance of arc plasma in the hybrid welding process of magnesium alloy. *Optics and Lasers in Engineering*, 47:1177–1182, 2009. (Cited page 3.)

[16] X. J. Cao, M. Jahazi, J. P. Immarigeon, and W. Wallace. A review of laser welding techniques for magnesium alloys. *Journal of Materials Processing Technology*, 171(2):188–204, 2006. (Cited page 3.)

[17] T. DebRoy and S. A. David. Physical processes in fusion welding. *Reviews of modern physics*, 67(1):85, 1995. (Cited pages 4 and 13.)

[18] A. N. Grezev. Plasma formation in laser welding. *Welding international*, 19(10):808–813, 2005. (Cited page 4.)

[19] S. Bannour, K. Abderrazak, H. Mhiri, and G. Le Palec. Effects of temperature-dependent material properties and shielding gas on molten pool formation during continuous laser welding of az91 magnesium alloy. *Optics & Laser Technology*, 44(8):2459–2468, 2012. (Cited page 4.)

[20] M. Capitelli, C. M. Ferreira, B. F. Gordiets, and A. I. Osipov. *Plasma kinetics in atmospheric gases*, volume 31. Springer Science & Business Media, 2013. (Cited page 4.)

[21] F. Hathat. Etude des vitesses de gaz de protection dans les dispositifs de soudage aux lasers de pièces d'alliages métalliques. *Mémoire de Master; Université de Ouargla*, 2017. (Cited page 4.)

[22] N. Guessoum and F. Benatallah. Echange de chaleur entre les gaz de protection et les pièces d'alliages métalliques. *Mémoire de Master; Université de Ouargla*, 2018. (Cited page 4.)

[23] M. Cvejić, M. R. Gavrilović, S. Jovićević, and N. Konjević. Stark broadening of mg i and mg ii spectral lines and debye shielding effect in laser induced plasma. *Spectrochimica Acta Part B: Atomic Spectroscopy*, 85:20–33, 2013. (Cited pages 4 and 18.)

[24] V. K. Unnikrishnan, K. Alti, V. B. Kartha, C. Santhosh, G. P. Gupta, and B. M. Suri. Measurements of plasma temperature and electron density in laser-induced copper plasma by time-resolved spectroscopy of neutral atom and ion emissions. *Pramana*, 74(6):983–993, 2010. (Cited page 4.)

[25] Y. Ben Nana. Etude spectroscopique des élargissements doppler des plasmas lors de la soudure aux lasers. *Mémoire de Master; Université de Ouargla*, 2015. (Cited page 4.)

[26] R. Bekhouche. Elargissement électronique des raies spectrales lors de soudure aux lasers. *Mémoire de Master; Université de Ouargla*, 2016. (Cited page 4.)

[27] D. E. Zenkhri. Calcul des éléments dipolaires électriques des structures atomiques: Application aux calculs des élargissements électroniques. *Mémoire de Master; Université de Ouargla*, 2019. (Cited page 4.)

[28] I. B. Gornushkin, L. A. King, B. W. Smith, N. Omenetto, and J. D. Winefordner. Line broadening mechanisms in the low pressure laser-induced plasma. *Spectrochimica Acta Part B: Atomic Spectroscopy*, 54(8):1207–1217, 1999. (Cited pages 4 and 30.)

[29] N. Konjević. Plasma broadening and shifting of non-hydrogenic spectral lines: present status and applications. *Physics reports*, 316(6):339–401, 1999. (Cited page 4.)

[30] D. Go. Gaseous ionization and ion transport: An introduction to gas discharges. *Department of Aerospace and Mechanical Engineering University of Notre Dame*, 2012. (Cited pages 5 and 13.)

[31] J. Hugill and T. Saktioto. A simplified chemical kinetic model for slightly ionized, atmospheric pressure nitrogen plasmas. *Plasma Sources Science and Technology*, 10(1):38, 2001. (Cited pages 6, 7, 10, and 24.)

[32] P. W. Atkins and J. De Paula. *Physical chemistry*. Oxford university press, 2010. (Cited pages 6 and 10.)

[33] C. S. Corr, S. Gomez, and W. G. Graham. Discharge kinetics of inductively coupled oxygen plasmas: experiment and model. *Plasma Sources Science and Technology*, 21(5):055024, 2012. (Cited page 6.)

[34] O. Eichwald, M. Yousfi, A. Hennad, and M. D. Benabdessadok. Coupling of chemical kinetics, gas dynamics, and charged particle kinetics models for the analysis of no reduction from flue gases. *Journal of applied physics*, 82(10):4781–4794, 1997. (Cited page 6.)

[35] N. Metropolis, A. W. Rosenbluth, A. H. Teller M. N. Rosenbluth, and E. Teller. Equation of state calculations by fast computing machines. *J. Chem. Phys*, 21:1087–1092, 1953. (Cited page 7.)

[36] H. C. Andersen. Molecular dynamics simulations at constant pressure and/or temperature. *The Journal of chemical physics*, 72(4):2384–2393, 1980. (Cited page 7.)

[37] F. Khelfaoui and O. Babahani. How to use the monte carlo simulation technique? application: A study of the gas phase during thin film deposition. In *Theory and Applications of Monte Carlo Simulations*. IntechOpen, 2019. (Cited page 7.)

[38] O. Babahani. Simulation numérique par la méthode de monte carlo de la déposition de couches minces par procédés cvd. *Thèse de doctorat; Université de Ouargla*, 2013. (Cited page 7.)

[39] T. J. Sommerer and M. J. Kushner. Numerical investigation of the kinetics and chemistry of rf glow discharge plasmas sustained in he, n_2, o_2, he/n_2/o_2, he/cf_4/o_2, and sih_4/nh_3 using a monte

carlo-fluid hybrid model. *Journal of Applied Physics*, 71(4):1654–1673, 1992. (Cited pages 7 and 8.)

[40] Z. Ballah and F. Khelfaoui. Numerical modeling of the electrical properties plasma argon in a rf magnetron sputtering and with einstein's relation of electron diffusivity. *Journal of King Saud University-Science*, 2018. (Cited pages 7 and 24.)

[41] W. Yi-Nan, L. Yue, Z. Shu, and L. Guo-Qiang. Numerical study on the characteristics of nitrogen discharge at high pressure with induced plasma. *Chinese Physics B*, 21(7):075202, 2012. (Cited page 8.)

[42] S. Ji-zhong, T. Stirner, and W. De-zhen. A kinetic study of ozone and nitric oxides in dielectric barrier discharges for o2/nox mixtures. *Plasma Science and Technology*, 4(2):1227, 2002. (Cited page 9.)

[43] C. L. Da Silva and V. P. Pasko. Dynamics of streamer-to-leader transition at reduced air densities and its implications for propagation of lightning leaders and gigantic jets. *Journal of Geophysical Research: Atmospheres*, 118(24):13–561, 2013. (Cited page 9.)

[44] C. D. Pintassilgo, D. Marinov, O. Guaitella, and A. Rousseau. Gas temperature variation in millisecond pulsed discharges in air. *31st ICPIG*, pages 14–19, 2013. (Cited pages 9 and 10.)

[45] J. Bacri and S. Raffanel. Calculation of transport coefficients of air plasmas. *Plasma Chemistry and Plasma Processing*, 9(1):133–154, 1989. (Cited page 9.)

[46] E. A. Mason and S. C. Saxena. Approximate formula for the thermal conductivity of gas mixtures. *The Physics of Fluids*, 1(5):361–369, 1958. (Cited page 9.)

[47] V. Boronenkov and Y. Korobov. Fundamentals of arc spraying. *Physical and Chemical Regularities*, 2012. (Cited page 10.)

[48] M. Nicolet. The collision frequency of electrons in the ionosphere. *Journal of Atmospheric and Terrestrial Physics*, 3(4):200–211, 1953. (Cited pages 10, 11, and 13.)

[49] E. L. Cussler and E. L. Cussler. *Diffusion: mass transfer in fluid systems*. Cambridge University Press, 2009. (Cited pages 10 and 11.)

[50] G. J. Nienhuis, W. J. Goedheer, E. A. G. Hamers, W.G. J. H. M. Van Sark, and J. Bezemer. A self-consistent fluid model for radio-frequency discharges in sih 4–h 2 compared to experiments. *Journal of Applied Physics*, 82(5):2060–2071, 1997. (Cited pages 10, 12, 13, and 26.)

[51] V. Nehra, A. Kumar, and H. K. Dwivedi. Atmospheric non-thermal plasma sources. *International Journal of Engineering*, 2(1):53–68, 2008. (Cited pages 13, 14, and 15.)

[52] A. M. El Sherbini, A. A. S. Al Aamer, A. T. Hassan, and T. M. El Sherbini. Measurements of plasma electron temperature utilizing magnesium lines appeared in laser produced aluminum plasma in air. *Optics and Photonics Journal*, 2(04):278, 2012. (Cited pages 14, 15, and 20.)

[53] D. Lacroix. Etude spectroscopique des plasmas de soudage laser: application au transfert d'énergie. *Université Henri Poincare, Nancy 1.*, 1997. (Cited pages 14 and 19.)

[54] A. M. El Sherbini, H. Hegazy, and TH. M. El Sherbini. Measurement of electron density utilizing the hα-line from laser produced plasma in air. *Spectrochimica Acta Part B: Atomic Spectroscopy*, 61(5):532–539, 2006. (Cited pages 14, 15, 16, and 20.)

[55] A. M. El Sherbini and A. A. S. Al Aamer. Development of a simple software program used for evaluation of plasma electron density in libs experiments via spectral line shape analysis. *Journal of Signal and Information Processing*, 3(04):502, 2012. (Cited pages 14, 15, 19, and 20.)

[56] Y. Ben Nana, F. Khelfaoui, S. Douis, L. E Sadeghzadeh, and M. T. Meftah. Effect of the ions on the electron collision operator through electronic trajectory modification. *Atoms*, 7(3):77, 2019. (Cited pages 14, 34, and 37.)

[57] H. K. Chung, R. W. Lee, M. H. Chen, and Y. Ralchenko. The how to for flychk. 2008. (Cited pages 14, 15, 18, 30, 31, and 38.)

[58] F. Khelfaoui. *Cours de Physique Atomique.* Master de Physique; Université de Ouargla, 2013. (Cited pages 14 and 20.)

[59] J. L. Delcroix and A. Bers. *Plasmas physic. Volume 1.* 1994. (Cited page 15.)

[60] J. Cooper. Plasma spectroscopy. *Reports on Progress in Physics*, 29(1):35, 1966. (Cited page 16.)

[61] G. W. F. Drake. *Springer handbook of atomic, molecular, and optical physics.* Springer Science & Business Media, 2006. (Cited pages 16, 17, 18, and 19.)

[62] R. Fitzpatrick. *course on non-relativistic quantum mechanics.* The University of Texas at Austin, 2010. (Cited page 17.)

[63] C. Aragón and J. A. Aguilera. Characterization of laser induced plasmas by optical emission spectroscopy: A review of experiments and methods. *Spectrochimica Acta Part B: Atomic Spectroscopy*, 63(9):893–916, 2008. (Cited pages 18 and 38.)

[64] M. Gharavi and S. G. Buckley. Single diode laser sensor for wide-range h_2o temperature measurements. *Applied Spectroscopy*, 58(4):468–473, 2004. (Cited page 20.)

[65] Z. Zhang and F. Zhang. Spectral analysis of welding plasma of magnesium alloy using flux coated wire. *Materials transactions*, 50(8):1909–1914, 2009. (Cited page 20.)

[66] S. Lemkeddem, F. Khelfaoui, and O. Babahani. Calculation of energy lost by radiation and convection during laser welding of ta6v titanium alloy. *Journal of Theoretical and Applied Physics*, 12(2):113–120, 2018. (Cited pages 23 and 39.)

[67] D. Kuzmin. A guide to numerical methods for transport equations. *University Erlangen-Nuremberg*, page 24, 2010. (Cited page 25.)

[68] J. D. Hoffman. Numerical methods for engineers and scientists, second edition revised and expanded, by marcel dekker. *Inc. New York*, 2001. (Cited page 26.)

[69] M. S. Dimitrijević and N. Konjević. Stark broadening of isolated spectral lines of heavy elements in plasmas. *Journal of Quantitative Spectroscopy and Radiative Transfer*, 30(1):45–54, 1983. (Cited page 30.)

[70] M. Baranger. Atomic and molecular processes. *edited by DR Bates, Academic Press, New York*, 1962. (Cited page 31.)

[71] H. R. Griem, M. Baranger, A. C. Kolb, and G. Oertel. Stark broadening of neutral helium lines in a plasma. *Physical Review*, 125(1):177, 1962. (Cited pages 31, 33, 35, and 57.)

[72] H. R. Griem. Stark broadening of isolated spectral lines from heavy elements in a plasma. *Physical Review*, 128(2):515, 1962. (Cited pages 31 and 58.)

[73] J. C. Moreno, H. R. Griem, S. Goldsmith, and J. Knauer. Measurements of gain and line broadening in lithiumlike aluminum. *Physical Review A*, 39(11):6033, 1989. (Cited page 31.)

[74] S. Alexiou and Y. Maron. Theoretically based closed form formulas for the collision operator for isolated ion lines in the standard stark-broadening theory. *Journal of Quantitative Spectroscopy and Radiative Transfer*, 53(1):109–124, 1995. (Cited page 32.)

[75] C. Tix and G. Simon. A transport theoretical model of the keyhole plasma in penetration laser welding. *Journal of Physics D: Applied Physics*, 26(11):2066, 1993. (Cited page 34.)

[76] I. S. Gradshteyn and I. M. Ryzhik. Table of integrals, series and products. *New York: Academic Press,| c1994, 5th ed. completely reset, edited by Jeffrey, Alan*, 1994. (Cited page 37.)

[77] O. A. Bukin, I. V. Bazarov, A. Y. Maior, N. S. Bodin, A. A. Il'in, V. I. Tsarev, and V. D. Kiselev. Estimation of the fulfillment of the local thermodynamic equilibrium criterion for the plasma generated by laser pulses of various shapes at the surface of a solid target. *Russian physics journal*, 44(5):472–477, 2001. (Cited page 38.)

ديناميكية التلحيم بالليزر لصفيحة من خليط معدني و التعريض الإلكتروني

ملخص

نهتم في هذه الدراسة بخصائص وسط البلازما القريبة من سطح صفيحة خليط معدني من المغنيزيوم أثناء اللحام بالليزر. من أجل درجة حرارة سطح متغيرة مع الزمن معينةT_s. نقوم بحساب دوال التوزيع المكاني والزماني لدرجة الحرارة الإلكترونيةT_e ودرجة حرارة الغازT_g والكثافة الإلكترونية N_e وكثافتي الجزيئات المتعادلة N_2 وO_2 وكثافتي الأيونات N_2^+ و O_2^+ باستخدام نموذج الموائع أحادي البعد. النموذج يحتوي على مجموعة من معادلات حركية للغازات، لوصف تطور انتقال الحرارة عن طريق الحمل الحراري. تم نقوم بحل نظام– المعادلات لدرجة الحرارة للغاز ودرجة الحرارة الالكترونية وكثافة الأنواع في وقت واحد، وذلك باستخدام طريقة المخطط الاسي أو طريقة الفروق المحدودة (FDM) والطرق التكرارية.

التشخيص الطيفي لاستخدام الخطوط الطيفية يمكن أن يكون أداة مفيدة جدا لفهم الظواهر في البلازما. ويمكن لهذه الخطوط الطيفية ان تتسع وتتعرض من خلال تعريض ستارك (الإلكتروني والأيوني) أو لأسباب أخرى. قمنا باقتراح طريقة مبسطة لحساب مساهمة الإلكترونات في التعريض الطيفي باستخدام نظرية التصادم بالتأثير المباشر (impact theory). النموذج يعتمد على حالتين حديتين للسرعة المختزلة (v_c<1) و(v_c>1) . قمنا بحساب تعريض ستارك الإلكتروني لخطوط معزولة من عناصر ثقيلة غير هيدروجينية Be I و Mg I و Ca I. كانت نتائجنا متوافقة مع أعمال سابقة . عند التلحيم في الشروط المعينة، تكون الكثافة الإلكترونية في حدود $9x10^8$ cm^{-3} والحرارة في حدود 3000 K. يكون تعريض ستارك مهمل مقارنة بتعريض دوبلر؛ الخطوط المعزولة للمغنيزيوم تمثل أداة جيدة لتحديد حرارة الغاز.

الكلمات المفتاحية: نموذج الموائع، المخطط الأسي، طريقة الفروق المحدودة، التوزيع البعدي و الزمني، المزيج الغازي N_2/O_2، تعريض ستارك الالكتروني، نظرية التصادم بالتأثير المباشر، السرعة المختزلة، الانتقالات الطيفية ل MgI.

Hydrodynamique du soudage laser de plaques d'alliages métalliques et élargissement électronique

Résumé

Nous nous sommes intéressés aux propriétés du milieu plasma près de la surface de soudure lors du soudage au laser de plaques d'alliages métalliques de magnésium. Pour une température de surface dépendant du temps donnée T_S, nous calculons les distributions spatiales et temporelles de la température électronique T_e, de la température du gaz T_g, de la densité des électrons N_e, des densités des neutres N_2 et O_2 et des densités des ions N_2^+ et O_2^+ en utilisant le modèle fluide à une dimension (1D). Le modèle est un ensemble d'équations de dynamique des gaz décrivant le transfert de chaleur par convection. Les équations couplées pour les températures et les densités d'espèces ont été résolues simultanément, à l'aide de la Méthode du Schéma Exponentiel (Schéma SG) ou la Méthode des Différences Finies (FDM) et des méthodes itératives.

Le diagnostic par spectroscopie de raies spectrales peut être très utile pour comprendre les phénomènes dans les plasmas. Ces raies spectrales peuvent être élargies par l'élargissement Stark (électronique et ionique) ou par d'autres causes. Nous avons proposé une méthode simple pour le calcul de la contribution des électrons à l'élargissement en se basant sur la théorie de l'impact. Le modèle est basé sur les deux cas limites d'une vitesse réduite : pour (v_c < 1) et pour (v_c > 1). Nous avons calculé les largeurs Stark électroniques pour les

raies isolées des éléments non hydrogénoides Be I, Mg I, Ca I. Nos résultats sont en bon accord avec des travaux précédents. Pour les conditions de soudage considérées, la densité des électrons est d'environ $9x10^{8}$ cm^{-3} et la température des électrons est d'environ 3000 K. L'élargissement Stark est négligeable comparée a l'élargissement de Doppler; les profils des raies isolées de Mg I sont un bon outil pour évaluer la température du gaz.

Mots clef : Modèle fluide, Schéma Exponentiel, Méthode des Différences Finies, Distributions spatiales et temporelles, Mélange gazeux N_2/O_2, Elargissement Stark électronique, Théorie d'Impact, vitesse réduite, Transitions radiatives Mg I.

Hydrodynamics of laser welding of metal alloys plates and Electronic broadening

Abstract

We are interested on properties of the plasma medium near the weld surface during laser welding of magnesium metal alloys plates. For a given surface temperature depending in time T_S, we calculate spatial and temporal distributions of the electronic temperature T_e, of the gas temperature T_g, of the electron density N_e and of the neutral densities of N_2 and O_2 and of the ion densities of N_2^+ and O_2^+ using one dimensional (1D) fluid model. The model contains a set of gas dynamics equations, to describe the heat transfer by convection. The coupled equations for temperatures and species densities were solved simultaneously, using Exponential Scheme (SG Scheme) or Finite Differences Method (FDM) and iterative methods.

The spectroscopic diagnosis by spectral lines can be very useful tools for understanding phenomena in plasmas. These spectral lines can be broadened by Stark broadening (electronic and ionic) or by other causes. We propose a simple method for calculation the contribution of electrons to the broadening using impact theory. The model is based on two limits case of the reduced velocity: for ($v_c < 1$) and for ($v_c > 1$). We calculate electronic Stark widths for isolated lines of the non hydrogenic heavy element Be I, Mg I, Ca I. Our results are in good agreement with previous works. For the considered welding conditions, electron density is about 9×10^{8} cm^{-3} and electron temperature is about 3000 K. The Stark broadening is negligible comparing with Doppler broadening; and the profiles of isolated lines of Mg I will be a good tool to evaluate gas temperature.

Keywords: Fluid model, Exponential Scheme, Finite Differences Method, Spatial and temporal distributions, N_2/O_2 gas mixture, Electronic Stark broadening, Impact theory, reduced velocity, Mg I radiatives transitions.